Scalar Fields in Four-Dimensional CDT

四维因果量子动力学三角化中的标量场

Andrzej Görlich

安杰伊·格尔利希

Contents

目录

Abstract

The model of Causal Dynamical Triangulations (CDT) is a non-perturbative and background-independent approach to the quantum theory of gravity. It provides a lattice regularization of the formal gravitational path integral and is manifestly coordinate-free. The lack of a coordinate system is an alluring property from the point of view of General Relativity (GR). Nevertheless, it is often convenient to have coordinates. In this Chapter, we define a coordinate system using classical scalar fields taking values in a target space with a topology matching the toroidal topology of the underlying spacetime manifold. These coordinates are equivalent to harmonic coordinates developed in the context of GR. Using Monte Carlo computer simulations of the four-dimensional CDT model and the introduced coordinates, we examine the properties of the quantum geometry. Although a single configuration is not physical, its properties can be useful in understanding the details of geometric nature. Visualizations of geometries using scalar fields as coordinates reveal cosmic structures of voids and filaments surprisingly similar to those observed in the real Universe and show clear differences between the individual phases of the model. It is indeed nontrivial that these ideas can be applied to understanding structures that appear in highly irregular and fluctuating geometries. In the second part, we study the backreaction of dynamical matter fields on quantum geometries. The quantum universe has a spatial topology of a three-torus, and the matter fields are multicomponent scalar fields taking values in a torus with circumference δ in each spatial direction. For sufficiently large δ , the scalar field induces a phase transition in which the spacetime topology changes from toroidal to spherical. This discovery may have important implications for quantum universes with nontrivial topologies.

摘要

因果动态三角剖分 (CDT) 模型是一种研究引力量子理论的非微扰、背景独立方法。它为形式化引力路径积分提供了格点正则化，且天生不依赖坐标。从广义相对论 (GR) 的角度来看，没有坐标系统是一个吸引人的性质，但引入坐标通常也会带来便利。本章中，我们定义了一套由经典标量场构建的坐标系统，该标量场的取值目标空间拓扑与基础时空流形的环面拓扑匹配。这些坐标等价于广义相对论框架下发展出的调和坐标。我们利用四维 CDT 模型的蒙特卡洛计算机模拟和引入的这套坐标，检验了量子几何的性质。尽管单独一个构型并不具有物理性，但它的性质有助于理解几何本质的细节。用标量场作坐标对几何进行可视化，可以揭示出空洞与纤维构成的宇宙结构，该结构与我们在真实宇宙中观测到的结构惊人相似，还能清晰展现模型不同相之间的差异。这些思路可用于理解高度不规则且存在涨落的几何中出现的结构，这一点确实非同寻常。在本文第二部分，我们研究了动态物质场对量子几何的反作用。量子宇宙的空间拓扑为三维环面，物质场为多分量标量场，在每个空间方向上取值于周长为 δ 的环面。当 δ 足够大时，标量场会诱发相变，使时空拓扑从环面变为球面。这一发现可能对研究具有非平凡拓扑的量子宇宙具有重要意义。

A. Görlich (☑)

A. 戈尔利希 (☑)

Institute of Theoretical Physics, Jagiellonian University, Krakow, Poland

波兰克拉科夫雅盖隆大学理论物理研究所

Mark Kac Center for Complex Systems Research, Jagiellonian University, Krakow, Poland e-mail: andrzej.goerlich@uj.edu.pl

波兰克拉科夫雅盖隆大学马克·卡克复杂系统研究中心电子邮箱:andrzej.goerlich@uj.edu.pl

Keywords

关键词

Quantum gravity . Lattice gravity - Causal dynamical triangulations . Quantum geometry - Scalar fields

量子引力。格引力——因果动态三角剖分。量子几何——标量场

Introduction

引言

Any realistic quantum theory of gravity should encompass matter fields [1]. In this chapter we describe how to include classical and dynamical scalar fields in Causal Dynamical Triangulations (CDT). CDT is a lattice approach to quantum gravity, and it is particularly well suited for Monte Carlo (MC) simulations including

matter fields such as scalar fields. Classical scalar fields do not contribute to the action and, consequently, do not influence the underlying quantum geometry but can be used to study it. Dynamical scalar fields do contribute to the action and are minimally coupled to gravity, and therefore can have an impact on spacetime and the phase structure.

任何现实的引力量子理论都必须包含物质场 [1]。本章我们将介绍如何在因果动态三角剖分 (CDT) 中引入经典和动力学标量场。CDT 是量子引力的一种格点方法，尤其适合包含标量场这类物质场的蒙特卡洛 (MC) 模拟。经典标量场不会对作用量产生贡献，因此也不会影响基础量子几何，但可用于研究量子几何。动力学标量场会对作用量产生贡献，且与引力最小耦合，因此会对时空和相结构产生影响。

Causal dynamical triangulations For the sake of completeness, here we briefly introduce the four-dimensional model of Causal Dynamical Triangulations. For a more detailed description, the reader is referred to - Chaps. 73, "Lattice Quantum Gravity: EDT and CDT" and -82, "Semiclassical and Continuum Limits of Four-Dimensional CDT" and publications [2-4].

因果动态三角剖分为保证内容完整，我们在此简要介绍四维因果动态三角剖分模型。更详细的说明可参阅第 73 章“格点量子引力:EDT 与 CDT”、第 82 章“四维 CDT 的半经典与连续极限”以及文献 [2-4]。

The results obtained within the four-dimensional model of Causal Dynamical Triangulations are already very promising [5]. The model shows a dynamical emergence of a semiclassical background geometry, which is a solution to the classical Einstein's equations along with superimposed quantum fluctuations of the spatial volume described by a minisuperspace model. It should be emphasized that CDT is a non-perturbative model and does not put by hand any background geometry. This result is particularly important because it arises as a subtle interplay of the entropic nature of triangulations and the bare action. It is one of the most remarkable and nontrivial effects of the model: the entropy reconstructs the effective action of the minisuperspace model, stabilizing it by changing the sign of the conformal mode precisely in the way prescribed by Hartle and Hawking [6].

四维因果动态三角剖分模型得到的结果已经非常可观 [5]。该模型显示半经典背景几何可以动力学涌现，该几何是经典爱因斯坦方程的解，同时叠加了由超空间模型描述的空间体积量子涨落。需要强调的是，CDT 是一个非微扰模型，不会手动预设任何背景几何。这一结果尤为重要，因为它来自三角剖分的熵性质与裸作用量之间的微妙相互作用。这是该模型最引人注目的非平凡效应之一: 熵重构了超空间模型的有效作用量，并恰好按照 Hartle 和 Hawking[6] 提出的方式改变共形模的符号，从而稳定了有效作用量。

The model of Causal Dynamical Triangulations is a diffeomorphism-invariant and background-independent, and thus non-perturbative, approach to the problem of quantizing the gravitational field [2]. The formal gravitational path integral can be expressed as

因果动态三角剖分模型是一种微分同胚不变、背景独立的非微扰方法，用于解决引力场的量子化问题 [2]。形式化的引力路径积分可以表示为:

$$\mathcal{Z}_{\mathrm{QG}} = \int \mathcal{D}_{\mathcal{M}}\,[g]\, e^{iS_{EH}[g_{\mu\nu}]}. \tag{1}$$

The above continuum path integral over four-dimensional spacetime geometries [g], i.e., equivalence classes of metrics g with respect to the diffeomorphism group $Diff_{\mathcal{M}}$ on the spacetime manifold $\mathcal{M}$, is weighted by the classical Einstein-Hilbert action:

上述对四维时空几何 [g](即时空流形 $\mathcal{M}$ 上微分同胚群 $Diff_{\mathcal{M}}$ 对应的度规 g 等价类) 的连续路径积分，由经典爱因斯坦-希尔伯特作用量加权:

$$S_{EH}\left[g_{\mu v}\right]=\frac{1}{16\pi G}\int_{\mathcal{M}}\mathrm{d}^4x\sqrt{-\det g}\,(R-2\Lambda)\,, \tag{2}$$

where G and Λ are Newton’ s gravitational constant and the cosmological constant, respectively, and R denotes the Ricci scalar curvature.

其中 G 和 Λ 分别是牛顿引力常数和宇宙学常数，R 表示里奇标量曲率。

The Causal Dynamical Triangulations model provides a lattice regularization of the formal path integral (1) through a sum over the discrete set of all causal triangulations $\mathbb{T}$. A four-dimensional triangulation comprises glued together four-simplices, which are a generalization of triangles to four dimensions. Causal Dynamical Triangulations assume global hyperbolicity of the spacetime manifold, $\mathcal{M}=[0,1]\times\sum$, and impose a global proper-time foliation whose leaves $\sum$, called slices, are spatial three-dimensional Cauchy surfaces. A spatial slice is a triangulation of the manifold $\sum$ made up of equilateral tetrahedra and is indexed by a discrete time coordinate $t=1,\ldots,T$. Two successive slices are connected by four-simplices that form a slab. The foliation introduces a distinction between space-like links with length a_s and time-like links with length a_t . As shown in Fig. 1 (left), there are two types of simplices. The picture on the right illustrates the foliation structure. A $\{4,1\}$-simplex has four vertices in one spatial slice and one vertex in the next/previous slice (further separated into $(4,1)$ / $(1,4)$ types), while a $\{3,2\}$ -simplex has three vertices in one spatial slice and two vertices in the next/previous slice ($(3,2)-$ / $(2,3)$-simplex). The inside of each simplex is a flat subset of a four-dimensional Minkowski spacetime.

因果动态三角剖分模型通过对所有因果三角剖分 $\mathbb{T}$ 的离散集合求和，为形式化路径积分 (1) 提供了格点正则化。四维三角剖分由粘合在一起的四单形构成，四单形是三角形向四维的推广。因果动态三角剖分假设时空流形 $\mathcal{M}=[0,1]\times\sum$ 满足整体双曲性，并施加了整体固有时叶分结构，其叶层 $\sum$ 被称为切片，是空间三维柯西曲面。每个空间切片是由等边四面体构成的流形 $\sum$ 三角剖分，由离散时间坐标 $t=1,\ldots,T$ 标记。两个相邻切片通过四单形连接，形成一个层块。这种叶分结构区分了长度为 a_s 的类空链接和长度为 a_t 的类时链接。如图 1(左) 所示，单形分为两类。右图展示了叶分结构:$\{4,1\}$ 单形的四个顶点位于同一个空间切片，一个顶点位于相邻的上/下切片 (可进一步分为 $(4,1)$ / $(1,4)$ 种类型)；而 $\{3,2\}$ 单形的三个顶点位于同一个空间切片，两个顶点位于相邻的上/下切片 (即为 $(2,3)$ 单形 ($(3,2)-$ /)。每个单形内部都是四维闵氏时空的一个平坦子集。

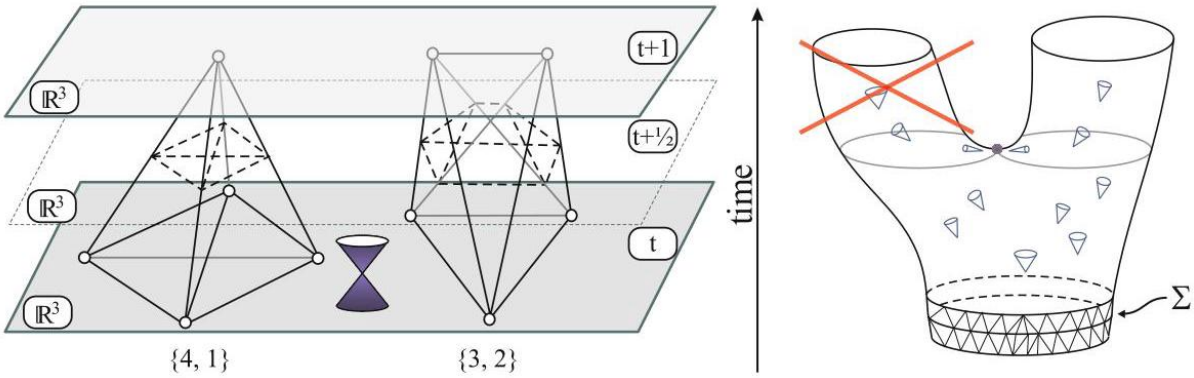

Fig. 1 Left: Visualization of two types of four-simplices, the fundamental building blocks of Causal Dynamical Triangulations. Simplices join two successive slices t and $t+1$. Right: An illustration of a two-dimensional triangulation with a light-cone structure and a branching point marked. In Causal Dynamical Triangulations, spatial slices $\sum$ are not allowed to split, which prevents singularities of the time arrow

图 1 左: 因果动态三角剖分的基本构造单元——两种四维单形的可视化。单形连接两个连续切片 t 和 $t+1$。右: 带有光锥结构的二维三角剖分示意图，标记出了一个分支点。在因果动态三角剖分中，不允许空间切片 $\sum$ 发生分裂，这避免了时间箭头的奇异性。

After applying the discretization procedure and the Wick rotation from Lorentzian to Euclidean signature [2], the path integral (1) becomes a partition function:

在完成离散化步骤并完成从洛伦兹号差到欧几里得号差的威克转动后 [2]，路径积分 (1) 变为配分函数:

$$\mathcal{Z}_{\mathrm{CDT}} = \sum_{\mathcal{T}\in\mathbb{T}} \frac{1}{C_{\mathcal{T}}} e^{-S_R[\mathcal{T}]} \tag{3}$$

where S_R is the Regge action and $C_{\mathcal{T}}$ is the symmetry factor, which is the order of the automorphism group of the triangulation $\mathcal{T}$ and might be viewed as the remnant of the volume of the diffeomorphism group. The discrete Regge action

其中 S_R 是里奇作用量，$C_{\mathcal{T}}$ 是对称因子，即三角剖分 $\mathcal{T}$ 自同构群的阶，可视为微分同胚群体积的残余。离散里奇作用量

$$S_R[\mathcal{T}] = -(k_0 + 6\Delta) N_0[\mathcal{T}] + k_4 (N_{41}[\mathcal{T}] + N_{32}[\mathcal{T}]) + \Delta N_{41}[\mathcal{T}] \tag{4}$$

is a piecewise-linear counterpart of the Einstein-Hilbert action (2), where k_0, k_4, and Δ are bare dimensionless coupling constants, related to the gravitational constant G, the cosmological constant Λ in (2), and the asymmetry factor a_t/a_s, respectively. N_0 denotes the number of vertices of a triangulation $\mathcal{T}$, N_{41} the number of $\{4,1\}$ - simplices, and N_{32} the number of $\{3,2\}$ -simplices.

是爱因斯坦-希尔伯特作用量 (2) 的分段线性对应形式，其中 k_0, k_4 、Δ 分别是无量纲裸耦合常数，分别对应 (2) 式中的引力常数 G 、宇宙学常数 Λ ，以及不对称因子 a_t/a_s 。N_0 表示三角剖分的顶点数，$\mathcal{T}, N_{41}$ 表示 $\{4,1\}$ 单形的数量，N_{32} 表示 $\{3,2\}$ 单形的数量。

Since the CDT model does not introduce any coordinates, such a formulation involves only geometric invariants, like lengths and angles, and is manifestly diffeomorphism-invariant (up to foliation). Let us emphasize that no ad hoc discreetness of spacetime is assumed from the outset, and the discretization appears only as a regularization. Finite lattice spacing a_s , i.e., the length of the spatial edges of the four-simplices, constitutes an ultraviolet cutoff, which is intended to be removed in the continuum limit $a_s \to 0$. The significance of lattice field theory as an underlying non-perturbative definition of continuum quantum field theory was highlighted by Wilson in [7].

由于 CDT 模型不引入任何坐标，该表述仅包含长度、角度这类几何不变量，且显然具有微分同胚不变性 (叶状结构除外)。需要强调的是，该模型从一开始就没有预先假定时空存在任何特设离散性，离散化仅作为正则化出现。有限格点间距 a_s 即四维单形空间边的长度，构成了紫外截断，该截断将在连续极限 $a_s \to 0$ 中被移除。威尔逊在文献 [7] 中指出了格点场论作为连续量子场论非微扰定义的重要意义。

Observables In order to study the phase structure or the underlying quantum geometries, we introduce observables, which can be measured on a triangulation and can serve as order parameters. Examples of observables are global parameters such as N_0, N_{41} , and N_{32} . Causal triangulations are equipped with a foliation that allows measuring the spatial three-volume n_t defined as the number of tetrahedra in a spatial slice t . It is the simplest observable that provides information about the geometry of the universe. The number of tetrahedra sums up to the total discrete volume $N_{41} = 2 \cdot \sum_{t=1}^{T} n_t$. Monte Carlo simulations of the four-dimensional CDT model generate four-dimensional triangulations according to the prescribed action, which then can be used to compute expectation values of observables or study individual configurations.

可观测量为了研究相结构与底层量子几何，我们引入可观测量: 可观测量可在三角剖分上测量，可作为序参量。可观测量的例子包括 N_0, N_{41} 和 N_{32} 这类全局参数。因果三角剖分带有叶状结构，可以测量定义为单个空间切片 t 内四面体数量的空间三体积 n_t 。这是最简单的可观测量，能够提供宇宙几何的相关信息。所有四面体的数量加总为总离散体积 $N_{41} = 2 \cdot \sum_{t=1}^{T} n_t$ 。四维 CDT 模型的蒙特卡洛模拟会按照给定作用量生成四维三角剖分，之后可用于计算可观测量的期望值或研究单个构型。

However, the aforementioned observables are quite coarse-grained. Although the CDT model is by construction diffeomorphism-invariant, it might be beneficial to introduce a natural coordinate system in order to explore and visualize geometric characteristics of a triangulation. In the following section, we describe how to implement harmonic coordinates via classical scalar fields on discrete triangulations.

但上述可观测量的粒度较粗。尽管 CDT 模型按构造本身就具有微分同胚不变性，引入自然坐标系仍有助于探索和可视化三角剖分的几何特征。在下一节中，我们将介绍如何通过离散三角剖分上的经典标量场实现调和坐标。

Topology The CDT model fixes the topology of spatial slices because topology changes are often associated with the violation of causality. For convenience, periodic boundary conditions in the time direction are

established, thus avoiding boundary terms, and the spacetime topology is $\mathcal{M} = S^1 \times \sum$.

拓扑 CDT 模型固定了空间切片的拓扑，因为拓扑变化通常与因果性破坏相关。为方便起见，我们在时间方向设置了周期性边界条件，从而避免了边界项，此时时空拓扑为 $\mathcal{M} = S^1 \times \sum$ 。

In the case of the spherical spatial topology $\left(\sum = S^3\right)$, there is a region of bare coupling constants, the so-called de Sitter phase, where volume profiles of typical configurations are not invariant under time translations, but are rather bell-shaped. The volume profile of a typical configuration in this phase is shown in Fig. 2 (blue line). However, the Einstein-Hilbert action, and in consequence the Regge action, has the time-translation symmetry. For time-periodic boundary conditions, a direct average $\langle n_t \rangle$ would give a constant function of time t , without capturing the shape of individual configurations. Therefore, to obtain a meaningful profile $\langle n_t \rangle$, the position of the center of volume of configurations is fixed before performing the average over triangulations [5, 8] . As shown in Fig. 2 (red line), the average profile $\langle n_t \rangle$ measured in the de Sitter phase is given by a cosine-cubed function. This profile corresponds to a semiclassical de Sitter background geometry (four-sphere), which emerges dynamically and is consistent with Einstein's equations [5]. Superimposed quantum fluctuations of the spatial volume are described by the minisuperspace model of Hartle and Hawking [6].

在球空间拓扑 $\left(\sum = S^3\right)$ 的情况下，存在一个裸耦合常数区域，即所谓的德西特相，其中典型构型的体积廓线不具有时间平移不变性，反而呈钟形。该相典型构型的体积廓线如图 2 蓝线所示。然而，爱因斯坦-希尔伯特作用量 (以及衍生的里奇作用量) 具有时间平移对称性。对于时间周期性边界条件，直接平均 $\langle n_t \rangle$ 会得到关于时间的常数函数 t ，无法捕捉单个构型的廓形。因此，为了得到有意义的廓线 $\langle n_t \rangle$ ，需要在对三角剖分求平均 [5, 8] 之前固定构型体积中心的位置。如图 2 红线所示，在德西特相测得的平均廓线 $\langle n_t \rangle$ 符合余弦三次方函数。该廓线对应动态涌现的半经典德西特背景几何 (四维球面)，符合爱因斯坦方程 [5]。空间体积的叠加量子涨落由哈特-霍金超空间模型描述 [6]。

The results suggest that there is also a semiclassical phase C for the toroidal spatial topology $\left(\sum = T^3\right)$, similar to the de Sitter phase for the spherical topology. Indeed, in this phase, a semiclassical background geometry emerges dynamically; however, it is completely different from the geometry for spherical topological conditions. In the toroidal case, the average volume profile $\langle n_t \rangle$ is no longer bell-shaped, but is a constant function of time t [9]. A typical volume profile n_t for the toroidal spatial topology is shown as a green line in Fig. 2. It oscillates around the average volume $\langle n_t \rangle$ whose value is constant in time and equal to $\frac{N_{41}}{T}$ (red line). The difference in the average volume profiles between the two topologies can be explained by studying the effective action and the minisuperspace model [10]. In this chapter a toroidal spatial topology will be assumed, i.e., $\sum = T^3$.

研究结果表明，环形空间拓扑 C 也存在半经典相 $\left(\sum = T^3\right)$ ，这与球拓扑的德西特相类似。事实上，该相中会动态涌现出半经典背景几何；但它与球拓扑条件下的几何完全不同。在环形情形中，平均体积轮廓 $\langle n_t \rangle$ 不再呈钟形，而是关于时间 t 的常函数 [9]。环形空间拓扑的典型体积轮廓 n_t 如图 2 中绿线所示，它在平均体积 $\langle n_t \rangle$ 附近振荡，该平均体积不随时间变化，大小等于 $\frac{N_{41}}{T}$ (红线)。两种拓扑之间平均体积轮廓的差异可以通过研究有效作用量和超空间最小化模型来解释 [10]。本章将假设空间拓扑为环形，即 $\sum = T^3$ 。

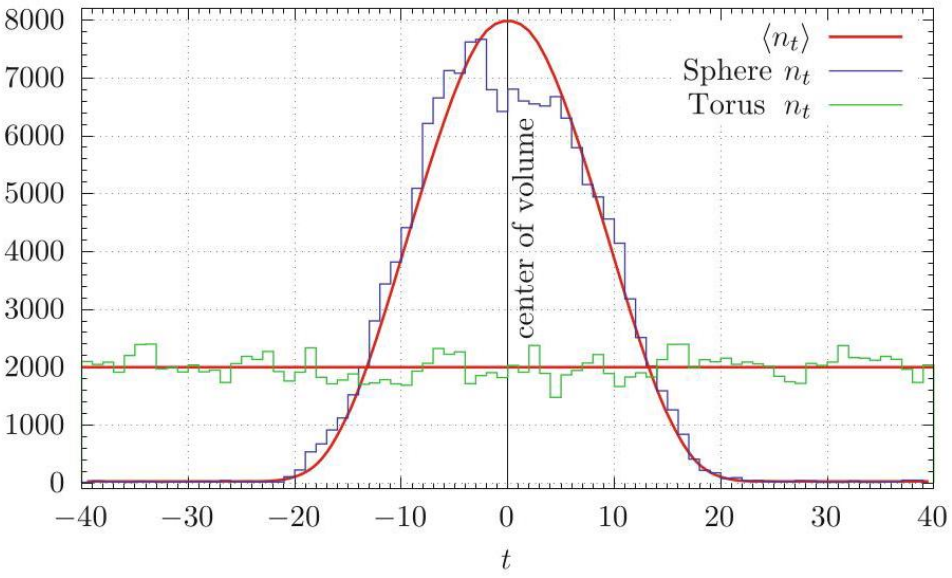

Fig. 2 Spatial volume profile n_t measured for a typical CDT configuration in the semiclassical phase C ($k_0 = 2.2, \Delta = 0.6, N_{41} = 160,000, T = 80$) with spherical spatial topology (blue) and toroidal spatial topology (green). Thick red lines denote average volume profiles $\langle n_t \rangle$ for both topologies

图 2 半经典相 C ($k_0 = 2.2, \Delta = 0.6, N_{41} = 160,000, T = 80$ 中典型 CDT 构型测得的空间体积廓线 n_t : 球空间拓扑 (蓝色) 与环面空间拓扑 (绿色)。粗红线表示两种拓扑的平均体积廓线 $\langle n_t \rangle$

Phase structure The Regge action (4) has three bare coupling constants k_0, k_4 , and Δ . The cosmological constant k_4 acts as a Lagrange multiplier and needs to be tuned to its critical value in order to keep the total four-volume N_4 fluctuating around some target value $\bar{N}_4$ during Monte Carlo simulations, leaving only the two coupling constants k_0 and Δ to be freely adjusted. The four-dimensional model of Causal Dynamical Triangulations has a rich phase structure consisting of four phases, A, B, C_b , and the semiclassical phase C [11-13]. Figure 3 presents the phase diagram in the plane spanned by k_0 and Δ . The phase diagram is based on Monte Carlo measurements for the toroidal spatial topology. Figure 4 shows spatial volume profiles n_t of generic CDT configurations in the four phases for the spherical (top) and toroidal (bottom) spatial topology.

相结构里奇作用量 (4) 包含三个裸耦合常数 k_0, k_4 和 Δ 。宇宙学常数 k_4 充当拉格朗日乘子，需要调谐至临界值，才能在蒙特卡洛模拟过程中让总四维体积 N_4 围绕某个目标值 $\bar{N}_4$ 涨落，仅剩下耦合常数 k_0 和 Δ 可以自由调整。四维因果动态三角剖分模型拥有丰富的相结构，共包含四个相: A, B, C_b 和半经典相 C [11-13]。图 3 给出了由 k_0 和 Δ 张成的平面内的相图，该相图基于环面空间拓扑的蒙特卡洛测量结果。图 4 展示了球空间拓扑 (上) 与环面空间拓扑 (下) 中，四个相内通用 CDT 构型的空间体积廓线 n_t 。

We observe four qualitatively different behaviors of a typical configuration depending on the values of the bare coupling constants k_0 and Δ :

根据裸耦合常数 k_0 和 Δ 取值的不同，我们观测到典型构型的四种定性不同行为:

Phase A. For large values of k_0 (see Fig.3), the universe disintegrates into uncorrelated irregular sequences of maxima and minima with time extent of a few steps. A number of universes oscillate along the

time direction. They are connected by necks of negligible sizes (see Fig. 4).

A 相。当 k_0 取值较大时 (见图 3)，宇宙分解为不相关的不规则极大、极小序列，时间跨度仅为几个步长。多个宇宙沿时间方向振荡，它们由尺寸可忽略的颈连接 (见图 4)。

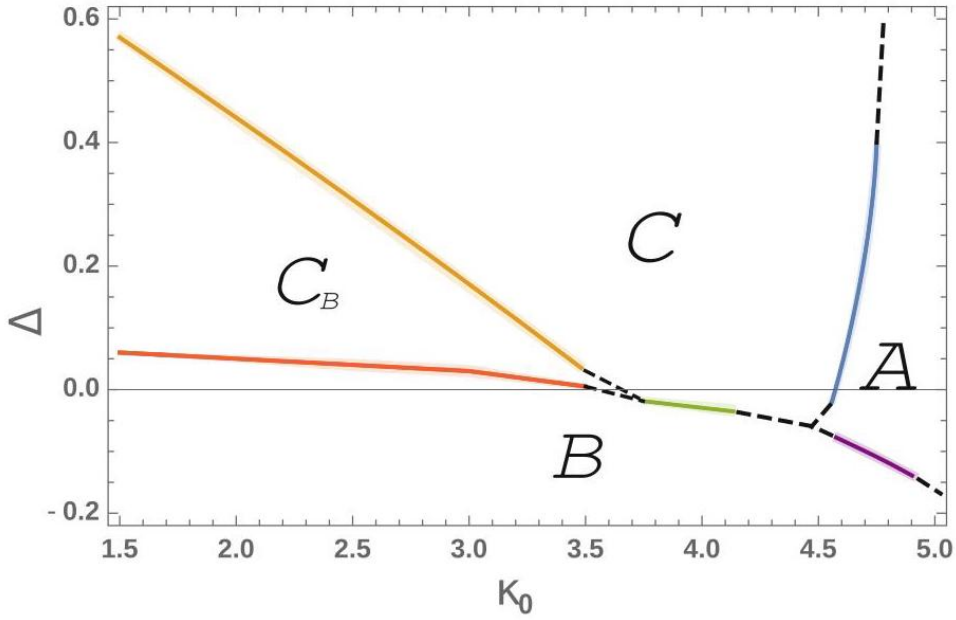

Fig. 3 Phase diagram of CDT with the four phases: A, B, C_b , and C . The plot shows the position of the phase transitions measured for the fixed lattice volume $\bar{N}_{41} = 160$k in the toroidal CDT

图 3 CDT 的相图，包含四个相: A, B, C_b 和 C 。图中标示了环形 CDT 中固定格点体积 $\bar{N}_{41} = 160$k 下测得的相变位置。

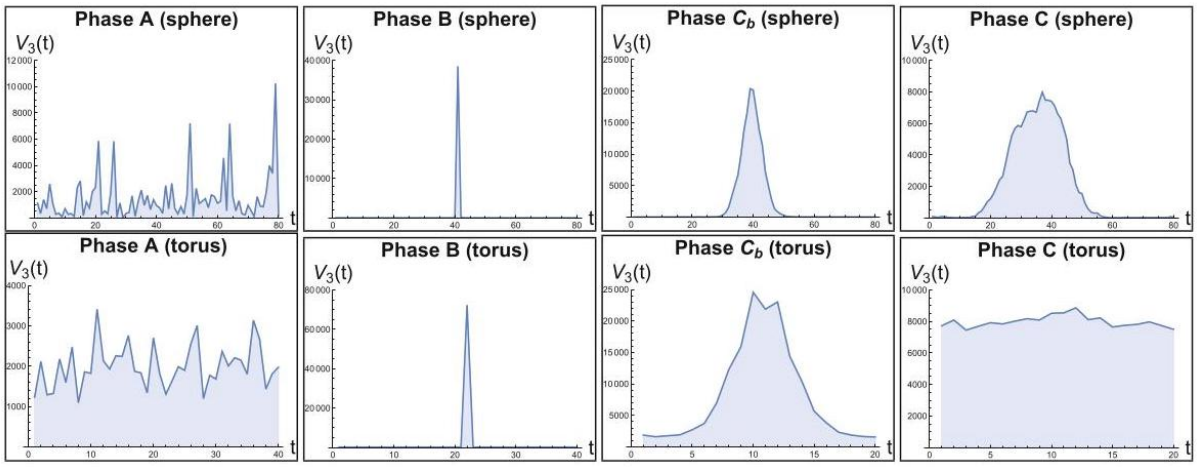

Fig. 4 Spatial volume profiles n_t of generic CDT configurations in phases A, B, C_b, C (from left to right) for spherical (top) and toroidal (bottom) spatial topology

图 4 球形 (上) 与环形 (下) 空间拓扑下，相 A, B, C_b, C 中典型 CDT 构型的空间体积剖面 n_t (从左至右)。

Phase B. For small values of Δ , nearly all simplices collapse into one spatial slice. Since the universe has neither time extent nor spatial extent, there is no geometry in a traditional sense.

B 相。当 Δ 取值较小时，几乎所有单纯形坍缩到同一个空间切片中。此时宇宙既没有时间延拓也没有空间延拓，不存在传统意义上的几何。

Phase $\mathbf{C_b}$. This phase, also called the bifurcation phase, was discovered during the research on the transfer matrix presented in the article [14]. Above some size of spatial volume, the ridge of the transfer matrix bifurcates into two branches. From the point of view of the spatial volume n_t , the properties are close to the semiclassical phase (cf. Fig. 4). However, in every second slice, we encounter singular high-order vertices.

$\mathbf{C_b}$ 相。该相也称为分岔相，是在研究本文 [14] 给出的转移矩阵时发现的。当空间体积大于某个尺度后，转移矩阵的脊分岔为两支。从空间体积 n_t 的性质来看，该相与半经典相接近 (参见图 4)，但每隔一个切片就会出现奇异的高阶顶点。

Phase C. The semiclassical phase is the most interesting from the physical point of view. In this phase, a semiclassical universe emerges dynamically with superimposed quantum fluctuations of the spatial volume. For spherical spatial topology, the Universe is a macroscopic four-dimensional (Euclidean) de Sitter space, and thus it is also called the de Sitter phase [5, 8]. The emergent background geometry behaves like a well-defined four-dimensional manifold, as measured by the spectral and Hausdorff dimensions, and with finite time and spatial extents. For the toroidal spatial topology, the average volume profile $\langle n_t \rangle$ is constant (see Fig. 4) [9].

C 相。半经典相是物理上最受关注的相。该相中，半经典宇宙动态涌现，空间体积存在叠加的量子涨落。对于球形空间拓扑，宇宙是宏观四维 (欧几里得) 德西特空间，因此该相也被称为德西特相 [5, 8]。通过谱维数和豪斯多夫维数测量可知，涌现的背景几何表现为一个定义良好的四维流形，具有有限的时间延拓和空间延拓。对于环形空间拓扑，平均体积剖面 $\langle n_t \rangle$ 为常数 (见图 4)[9]。

For a more detailed description of the phase diagram and the phases themselves, the reader is referred to Chap. 82, ”Semiclassical and Continuum Limits of Four-Dimensional CDT” and article [15]. In the next section, a coordinate system will be defined on CDT triangulations, which will allow for visualization of the configurations. The pictures will show a clear distinction between the different phases. In section ”Dynamical Scalar Fields,” a backreaction of dynamical scalar fields on configurations in the semiclassical phase C will be discussed.

关于相图和各相的更详细描述，读者可参考第 82 章“四维 CDT 的半经典极限与连续极限”和文献 [15]。下一节我们会在 CDT 三角剖分上定义坐标系，实现对构型的可视化，图像将清晰展示不同相之间的区别。在“动力学标量场”一节，我们将讨论动力学标量场对半经典相 C 中构型的反作用。

Classical Scalar Fields

经典标量场

The model of Causal Dynamical Triangulations is manifestly coordinate-free and thus diffeomorphism-invariant. The lack of a coordinate system is an attractive property from the perspective of General Relativity (GR). Nonetheless, it is often convenient to have a coordinate system at one's disposal in order to examine features of quantum geometries. Although, given a triangulation, a geometry together with a coordinate system may be reconstructed from the relations between four-simplices, here, a different approach will be considered. To define coordinates, we will use matter fields, which will play the role of dynamical reference clock-and-rods fields. This concept is well established in many approaches to gravity [16,17]. Typical quantum CDT configurations that contribute to the path integral have a highly fractal character. To explore the geometric characteristics of such triangulations, it would be beneficial to have a natural coordinate system [18].

因果动态三角剖分模型具有明显的无坐标特性，因此是微分同胚不变的。从广义相对论 (GR) 的角度来看，缺乏坐标系是一个吸引人的性质。尽管如此，为了研究量子几何的特征，手头拥有坐标系通常更为方便。虽然给定一个三角剖分，我们可以通过四胞体之间的关系重构出几何与坐标系，但本文将采用一种不同的方法。为了定义坐标，我们将使用物质场，它们会充当动力学参考钟尺场的角色。这一概念在许多引力研究方法中都已经得到了成熟的应用 [16,17]。对路径积分有贡献的典型量子 CDT 构型具有高度分形特征。为了探究这类三角剖分的几何特性，拥有一个自然坐标系会很有帮助 [18]。

We will start with a continuum description of the procedure for adding scalar fields, which will later serve as a coordinate system, to a four-dimensional CDT configuration with topology $T^4 = S^1 \times S^1 \times S^1 \times S^1$. Let $\mathcal{M}$ be a Riemannian manifold with the topology of T^4 equipped with a metric $g_{\mu\upsilon}$. The aim is to construct a good nontrivial harmonic map from $\mathcal{M}$ to T^4 equipped with a trivial flat metric $\delta_{\mu\upsilon}$. Let us define a set of four scalar fields $\phi^\sigma, \sigma = 1, 2, 3, 4$, each being a map $\mathcal{M} \to S^1$ that minimizes the action:

我们首先用连续语言描述如何将后续用作坐标系的标量场添加到拓扑为 $T^4 = S^1 \times S^1 \times S^1 \times S^1$ 的四维 CDT 构型中。设 $\mathcal{M}$ 为具有 T^4 拓扑、配有度规 $g_{\mu\upsilon}$ 的黎曼流形。我们的目标是构造一个良好的非平凡调和映射，从 $\mathcal{M}$ 映射到配有平凡平坦度规 $\delta_{\mu\upsilon}$ 的 T^4。我们定义一组四个标量场 $\phi^\sigma, \sigma = 1, 2, 3, 4$，每个都是最小化该作用量的映射 $\mathcal{M} \to S^1$：

$$S_M[\phi] = \frac{1}{2}\int \mathrm{d}^4x\sqrt{g(x)}g^{\mu\upsilon}(x)\,\partial_\mu\phi^\sigma(x)\,\partial_\upsilon\phi^\sigma(x). \tag{5}$$

Due to the trivial metric on the target manifold T^4, the action (5) decouples into four equations for each direction σ, and fields $\phi^\sigma(x)$ can be treated separately. Let $\phi(x)$ be a harmonic map $\mathcal{M} \to S^1$ that minimizes the action (5), then it satisfies the Laplace equation:

由于目标流形 T^4 上是平凡度规，作用量 (5) 可以解耦为每个方向 σ 对应的四个独立方程，因此可以分开处理场 $\phi^\sigma(x)$。设 $\phi(x)$ 是最小化作用量 (5) 的调和映射 $\mathcal{M} \to S^1$，则它满足拉普拉斯方程:

$$\Delta\phi(x) = 0,\ \phi(x) \in S^1, \tag{6}$$

where

其中

$$\Delta = \frac{1}{\sqrt{g(x)}} \frac{\partial}{\partial x^{\mu}} \left(\sqrt{g(x)} g^{\mu v}(x) \right) \frac{\partial}{\partial x^{v}}.$$

The topology S^1 of the target space is significant, since if the scalar field $\phi(x)$ were taking values in $\mathbb{R}$, then the constant mode would be the only solution on a compact manifold $\mathcal{M}$. Clearly, such a trivial solution is not an interesting one, but there are other possibilities. Let the circumference of S^1 be δ. For technical reasons, the $\phi(x)$ field is let to have values in $\mathbb{R}$, but to implement $\phi(x) \in S^1(\delta)$, values $\phi(x)$ and $\phi(x) + n \cdot \delta, n \in \mathbb{Z}$, are identified, leading to a mapping

目标空间的拓扑 S^1 非常重要，因为如果标量场 $\phi(x)$ 的取值在 $\mathbb{R}$ 中，那么紧致流形 $\mathcal{M}$ 上只有常数模是解。显然这种平凡解没有研究意义，但还存在其他可能。设 S^1 的周长为 δ。出于技术原因，我们允许 $\phi(x)$ 场的取值范围为 $\mathbb{R}$，但为了实现 $\phi(x) \in S^1(\delta)$，我们将 $\phi(x)$ 和 $\phi(x) + n \cdot \delta, n \in \mathbb{Z}$ 等同起来，最终得到一个映射

$$\mathbb{R} \ni \phi \to \psi = \frac{\delta}{2\pi} \mathrm{e}^{2\pi \mathrm{i} \phi / \delta} \in S^1(\delta). \tag{7}$$

In the simple case $\mathcal{M} = S^1$, a function

在简单情形 $\mathcal{M} = S^1$ 下，函数

$$\phi(x) = k \cdot x + \text{ const.}, \ x \in [0, \delta), \ k \in \mathbb{Z}, \tag{8}$$

is a harmonic map $S^1 \to S^1$ and a solution to (6) that winds k times around S^1 with circumference δ. Solutions with different k cannot be continuously transformed into each other.

是调和映射 $S^1 \to S^1$，也是方程 (6) 的解，它绕周长为 δ 的 S^1 缠绕 k 圈。具有不同 k 的解无法连续变换到彼此。

Given a four-dimensional triangulation, there is an associated dual graph, where a vertex corresponds to a four-simplex in the triangulation, and an edge corresponds to a connection between two adjacent four-simplices. Every simplex in a four-dimensional triangulation has exactly five neighbors; thus, the dual graph is an undirected five-valent graph where centers of four-simplices are connected by edges corresponding to tetrahedra shared by the joined simplices. In the case of Causal Dynamical Triangulations, the scalar field $\phi(x)$ can be discretized by placing it on the dual lattice and locating the field values ϕ_i inside four-simplices without differentiating between $\{4,1\}$ - and $\{3,2\}$ -simplices. The discrete counterpart of the continuous action (5) for a single field ϕ (component in a given direction) reads:

给定一个四维三角剖分，可得到与之对应的对偶图: 对偶图中一个顶点对应三角剖分中的一个四维单形，一条边对应两个相邻四维单形之间的连接。四维三角剖分中的每个单形恰好有五个邻接单形，因此对偶图是一个无向五价图，其中各四维单形的中心通过边连接，这些边对应被连接单形所共有的四面体。在因果动态三角剖分中，可将标量场 $\phi(x)$ 离散化: 把它放在对偶晶格上，将场值 ϕ_i 定位在四维单形内部，无需区分 $\{4,1\}$ 单形和 $\{3,2\}$ 单形。单个场 ϕ (给定方向上的分量) 对应的连续作用量 (5) 的离散形式如下:

$$S_M[\phi, \mathcal{T}] = \frac{1}{2} \sum_{i \leftrightarrow j} (\phi_i - \phi_j)^2 = \sum_{i,j} \phi_i L_{ij} \phi_j = \phi^T \mathbf{L} \phi, \tag{9}$$

where the first sum is over all pairs of neighboring four-simplices, the second sum is over all four-simplices in the triangulation $\mathcal{T}$, and $\mathbf{L}$ is the discrete Laplacian matrix. In the four-dimensional case, matrix $\mathbf{L}$ is a $N_4 \times N_4$ symmetric matrix which can be expressed by the adjacency matrix $\mathbf{A}$ representing the dual graph:

其中第一个求和遍历所有相邻四维单形对，第二个求和遍历三角剖分 $\mathcal{T}$ 中的所有四维单形，且 $\mathbf{L}$ 是离散拉普拉斯矩阵。在四维情况下，矩阵 $\mathbf{L}$ 是一个 $N_4 \times N_4$ 对称矩阵，可由表示对偶图的邻接矩阵 $\mathbf{A}$ 表示为:

$$\mathbf{L} = 5\mathbb{1} - \mathbf{A} \tag{10}$$

where N_4 is the number of vertices in the dual lattice, i.e., the total number of four-simplices in the original triangulation, and1is the $N_4 \times N_4$ unit matrix. The adjacency matrix $\mathbf{A}$ of the dual graph is defined as

其中 N_4 是对偶晶格的顶点数，即原三角剖分中四维单形的总数，1 是 $N_4 \times N_4$ 单位矩阵。对偶图的邻接矩阵 $\mathbf{A}$ 定义为

$$A_{ij} = \begin{cases} 1 & \text{if link } (i,j) \text{ belongs to the dual lattice,} \\ 0 & \text{otherwise.} \end{cases} \tag{11}$$

A field ϕ_i which minimizes the action (9) and takes values in $\mathbb{R}$ fulfills the discrete Laplace equation:

使作用量 (9) 取极小值、且取值在 $\mathbb{R}$ 中的场 ϕ_i 满足离散拉普拉斯方程:

$$\mathbf{L}\phi = 0. \tag{12}$$

For a finite triangulation of a closed manifold, the Laplacian matrix has only one zero mode, which is a constant vector $\phi_i = \text{const}$.

对于闭流形的有限三角剖分，拉普拉斯矩阵仅有一个零模，即常矢量 $\phi_i =$ $ \text{const.}$

However, as stated before, we are interested in nontrivial solutions where the field ϕ_i minimizes the action (9) under the constraint that $\phi_i \in S^1$ winds around S^1 once. This constraint requires special care when implemented on a discrete triangulation of the manifold $\mathcal{M} = T^4$. To achieve that ϕ_i winds once around S^1 , we construct a set of four nonequivalent three-dimensional closed hypersurfaces, i.e., hypersurfaces that cannot be continuously transformed into another, consisting of tetrahedral faces of four-simplices. Each hypersurface has a topology of T^3 and is intersected exactly once by one of the four independent non-contractible loops winding around the toroidal CDT triangulation $\mathcal{T}$. The choice of a toroidal spatial topology seems convenient for this purpose. Contrary to the spherical topology, one can define three-dimensional hypersurfaces, called boundaries, which are orthogonal to each other and non-contractible. See Fig. 5 for a two-dimensional visualization of a manifold with boundaries. For more information on how to impose such hypersurfaces on a CDT triangulation, see [19, 20]. Let us consider one of the closed hypersurfaces, and let the field ϕ_i jump by δ when crossing the hypersurface. This is exactly what happened in the continuum solution (8) for $k = 1$.

The discontinuity of the field ϕ_i along the hypersurface is virtual and is not present when the field is viewed as belonging to S^1 . For the same reason, the hypersurface itself is not physical, since it cannot be identified when expressing ϕ_i as a field with values in S^1 .

但如前所述，我们关注的是非平凡解: 在 $\phi_i \in S^1$ 绕 S^1 一周的约束下，场 ϕ_i 使作用量 (9) 取极小值。在流形 $\mathcal{M} = T^4$ 的离散三角剖分上实现该约束时需要特殊处理。为了让 ϕ_i 绕 S^1 一周，我们构造了四个不等价的三维闭超曲面，即无法连续变形为彼此的超曲面，它们由四维单形的四面体面组成。每个超曲面都具有 T^3 拓扑，恰好被环绕环形 CDT 三角剖分 $\mathcal{T}$ 的四个独立不可收缩环路中的一个相交一次。对于该构造，选择环形空间拓扑十分方便。与球面拓扑不同，我们可以在环形拓扑中定义两两正交、不可收缩的三维超曲面 (称为边界)。关于带边界流形的二维可视化参见图 5。关于如何在 CDT 三角剖分上引入这类超曲面的更多信息参见文献 [19, 20]。考虑其中一个闭超曲面，当穿过该超曲面时，场 ϕ_i 发生 δ 的跳跃。这正是 $k = 1$ 的连续解 (8) 中的情况。沿超曲面的场 ϕ_i 不连续性是虚拟的: 当场被视为属于 S^1 的场时，该不连续性不存在。同理，超曲面本身也不是物理的，因为将 ϕ_i 表示为取值在 S^1 中的场时，无法识别出该超曲面。

We tentatively view ϕ_i as an ordinary scalar field in $\mathbb{R}$ with a jump at the hypersurface. This setup ensures that there is a unique solution which minimizes the action (9) and is orthogonal to the constant mode. By construction, the field ϕ_i is stretched by δ when moving along any of the non-contractible loops which intersects the hypersurface once. This construction is applied separately to each of the four nonequivalent and non-contractible loops in the triangulation $\mathcal{T}$, so that there are four scalar fields $\left(\phi_i^x, \phi_i^y, \phi_i^z, \phi_i^t\right)$, which provide a map $\mathcal{T} \to S^1 \times S^1 \times S^1 \times S^1$ and which will serve as coordinates. It should be noted that coordinate systems defined in such a way are different for different configurations contributing to the path integral.

我们暂时将 ϕ_i 视为 $\mathbb{R}$ 中的普通标量场，它在超曲面上存在跃变。该设置可保证存在唯一解，能使作用量 (9) 最小化，且与常数模正交。根据构造，当 ϕ_i 场沿任意一条与超曲面相交一次的不可收缩环路移动时，会被 δ 拉伸。该构造分别应用于三角剖分 $\mathcal{T}$ 中四条不等价的不可收缩环路，因此得到四个标量场 $\left(\phi_i^x, \phi_i^y, \phi_i^z, \phi_i^t\right)$ ，它们给出一个映射 $\mathcal{T} \to S^1 \times S^1 \times S^1 \times S^1$ ，并将用作坐标。需要注意的是，如此定义的坐标系，对路径积分中不同的贡献构型是不同的。

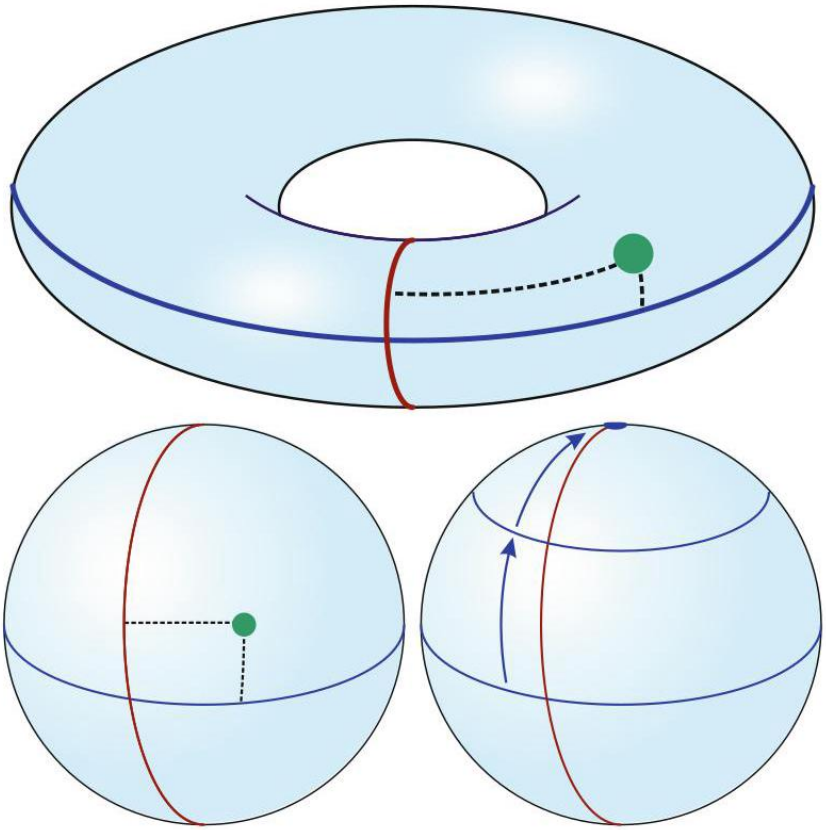

Fig. 5 In the two-dimensional toroidal case, two orthogonal non-contractible loops can be constructed and used to define coordinates (top chart). This is not possible in a spherical case, where all loops are contractible to a point (bottom chart)

图 5 在二维环面情形，可以构造两个正交的不可收缩环路，并用它们定义坐标 (上图)。这在球面情形无法实现，因为球面中所有环路都可收缩为一个点 (下图)

Scalar Fields as Coordinates

标量场作为坐标

The jump condition Given an oriented three-dimensional boundary or hypersurface defined as a non-contractible connected subset of tetrahedra (faces of four-simplices), the field ϕ_i in a simplex i adjacent to the boundary will perceive the value of the field ϕ_j in a simplex j on the other side of the boundary as shifted by $+\delta$ or $-\delta$ depending on the orientation of the boundary. In the dual-graph picture, a boundary is a subset of dual links. See [19, 20] for an explicit construction of relevant boundaries and Fig. 6 for a two-dimensional illustration of a triangulation with a boundary, where the field jumps when crossing it. The figure at the bottom presents a boundary shift together with a corresponding field redefinition (black triangle).

跃变条件给定一个定向三维边界或超曲面，它被定义为不可收缩的连通四面体 (四单纯形的面) 集合，毗邻该边界的单纯形 i 中的场 ϕ_i 会发现，边界另一侧单纯形 j 中的场 ϕ_j 的值会根据边界的定向偏移 $+\delta$ 或 $-\delta$ 。在对偶图图像中，边界是对偶链接的一个子集。相关边界的显式构造参见 [19, 20] ，带边界三角剖分的二维示例参见图 6，穿越该边界时场会发生跃变。底部图给出了边界偏移及对应的场重定义 (黑色三角形)。

In the case of classical scalar fields, the exact value of the jump δ is not important because the solution scales trivially with the jump magnitude. Thus, for convenience, we will further take $\delta = 1$, remembering that it can always be reintroduced by rescaling $\phi_i \to \delta\phi_i$. One can define an antisymmetric jump matrix

对于经典标量场，跃变 δ 的精确取值并不重要，因为解会随跃变幅度简单缩放。因此为方便起见，我们后文直接取 $\delta = 1$ ，需要时总可以通过重新缩放 $\phi_i \to \delta\phi_i$ 将其还原。我们可以定义一个反对称跃变矩阵

$$B_{ij} = \begin{cases} +1 & \text{if the dual link } i \to j \text{ crosses} \\ & \text{the boundary in the positive direction,} \\ -1 & \text{if the dual link } i \to j \text{ crosses} \\ & \text{the boundary in the negative direction,} \\ 0 & \text{otherwise,} \end{cases} \tag{13}$$

Fig. 6 Top: An example of a two-dimensional triangulation with toroidal topology and an oriented boundary. The field value jumps by ±1 when crossing the boundary, the jump is compensated by the boundary term b in (15). A boundary might contain bubbles which push field values outside an interval of width 1. Bottom: A step of the boundary shift together with a corresponding field redefinition. The black triangle is flipped to the other side of the boundary and its field value is decreased by 1

图 6 顶部: 环面拓扑下带定向边界的二维三角剖分示例。穿越边界时场值跃变 ±1 ，该跃变由 (15) 式中的边界项 b 补偿。边界可能包含泡，将场值推出宽度为 1 的区间。底部: 一步边界偏移及对应的场重定义。黑色三角形被翻转到边界另一侧，其场值减小 1

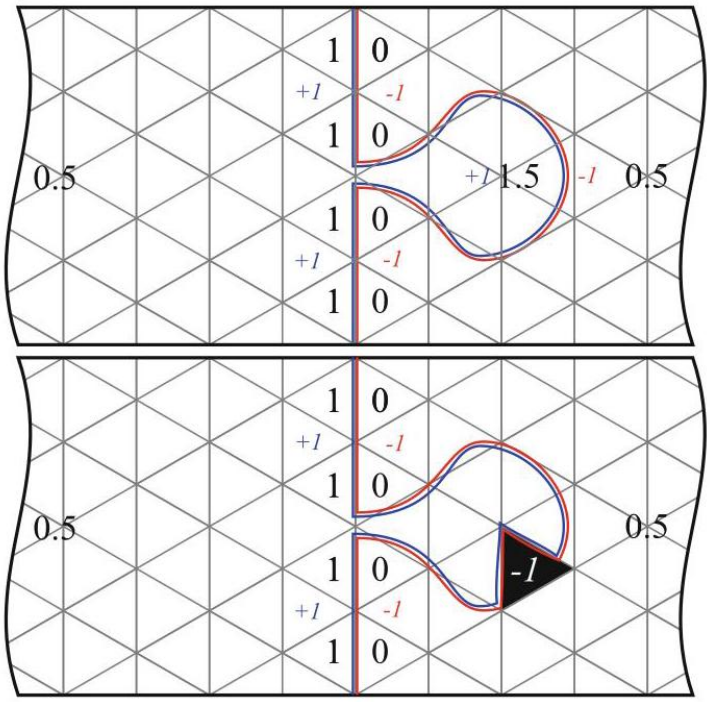

and a boundary (jump) vector

以及一个边界 (跃变) 向量

$$b_i = \sum_j B_{ij} \tag{14}$$

The modified version of the scalar field action (9) taking into account the jump of the field at the boundary is given by

考虑边界处场的跃变后，修正版的标量场作用量 (9) 由下式给出

$$S_M[\phi, \mathcal{T}] = \frac{1}{2}\sum_{i \leftrightarrow j}\left(\phi_i - \phi_j - B_{ij}\right)^2 = \sum_{i,j}\phi_i L_{ij}\phi_j - 2\sum_i \phi_i b_i + V$$

$$= \phi^T \mathbf{L}\phi - 2\phi^T b + V \tag{15}$$

where V is the three-volume of the boundary, i.e., the number of tetrahedra belonging to the boundary:

其中 V 是边界的三维体积，即属于该边界的四面体数量:

$$V = \frac{1}{2}\sum_{i,j} B_{ij}^2 = \frac{1}{2}\sum_i |b_i| \,. \tag{16}$$

The jump matrix $\mathbf{B}$ compensates for the jump $\delta = 1$ of the scalar field at the boundary.

跃变矩阵 $\mathbf{B}$ 补偿标量场在边界处的跃变 $\delta = 1$ 。

In (16) we used the fact that the boundary vector b_i measures the number of tetrahedral faces that a particular four-simplex i has on the boundary and b_i is an integer in the range $-5 \leq b_i \leq 5$. As in the case without a jump, the action (15) is invariant under a constant shift in the scalar field values (the Laplacian zero mode). It is also invariant under simultaneous boundary shift and a corresponding field redefinition in such a way that the field is not altered when viewed as taking values on S^1 , see Fig. 6 (bottom).

在 (16) 式中我们利用了这一性质: 边界向量 b_i 度量给定四单纯形 i 位于边界上的四面体面的数量, 因此 b_i 是属于区间 $-5 \leq b_i \leq 5$ 的整数。和无跃变的情况一样，作用量 (15) 在标量场值整体平移 (拉普拉斯零模) 下不变。它同时在边界平移和对应场重定义下不变，此时场视作定义在 S^1 上的取值不发生改变，参见图 6(底部)。

The classical solution A classical solution for ϕ_i minimizes the action (15) and satisfies the discrete Laplace equation with a boundary term:

经典解 ϕ_i 的经典解使作用量 (15) 取极小值，且满足带边界项的离散拉普拉斯方程:

$$\mathbf{L}\phi = b. \tag{17}$$

Formally, the above equation is a Poisson equation; however, we will call it the Laplace equation, since b is not a source term when we view the field as a field with values in S^1 . Due to the translational symmetry of the action under a constant shift of the field, a constant vector is a zero mode of the Laplacian matrix $\mathbf{L}$, and consequently $\mathbf{L}$ is not invertible. Nonetheless,(17) has a solution as long as the jump vector b is orthogonal to the zero mode, which is exactly the case $\left(\sum_i b_i = \sum_{i,j} B_{ij} = 0\right)$. A unique solution $\overline{\phi}$ to (17) is obtained by requiring that for some simplex with label i_1 the field value $\overline{\phi}_{i_1} = 0$. In this case, the solution can be formally written as

形式上，上述方程是泊松方程，但我们仍将其称为拉普拉斯方程，因为当我们把场视作取值在 S^1 上的场时，b 并非源项。由于作用量在场整体平移下具有平移对称性，常向量是拉普拉斯矩阵 $\mathbf{L}$ 的零模，因此 $\mathbf{L}$ 不可逆。尽管如此，只要跃变向量 b 与零模正交，方程 (17) 就存在解，而 $\left(\sum_i b_i = \sum_{i,j} B_{ij} = 0\right)$ 恰好满足这一条件。我们可以要求标号为 i_1 的某单纯形满足场值条件 $\overline{\phi}_{i_1} = 0$ ，从而得到 (17) 的唯一解 $\overline{\phi}$ 。此时解可以形式地写为

$$\overline{\phi} = \mathbf{L}^{-1}b,\ \overline{\phi}_{i_1} = 0. \tag{18}$$

The requirement $\overline{\phi}_{i_1} = 0$ can always be satisfied, since we are free to shift the field by a constant. It is feasible to numerically compute the classical solution, although technically challenging for large system sizes, $N_4 \sim 10^6$. For a description of the numerical algorithms used to solve this problem, we refer the reader to [21]. The four scalar fields $\overline{\phi}^{\mu}, \mu = x, y, z, t$, given by the solution (18) with the boundary vector b encoding a boundary orthogonal to the direction μ , provide the desired harmonic map $\mathcal{T} \to S^1 \times S^1 \times S^1 \times S^1$.

要求 $\overline{\phi}_{i_1} = 0$ 总能被满足，因为我们可以自由地给场平移一个常数。数值计算经典解是可行的，尽管对于大尺寸系统来说存在技术难点，$N_4 \sim 10^6$ 。关于求解该问题所用数值算法的说明，我们建议读者参阅文献 [21]。四个标量场 $\overline{\phi}^{\mu}, \mu = x, y, z, t$ 由式 (18) 的解给出，其中边界向量 b 编码了一个垂直于方向 μ 的边界，它们给出了我们所需的调和映射 $\mathcal{T} \to S^1 \times S^1 \times S^1 \times S^1$ 。

From (10) and (18), it follows that the classical solution $\overline{\phi}$ has a natural property:

由式 (10) 和式 (18) 可得，经典解 $\overline{\phi}$ 具备一个自然性质:

$$\overline{\phi}_i = \frac{1}{5}\left(b_i + \sum_{j \to i} \overline{\phi}_j\right), \tag{19}$$

meaning that for every simplex i , the field value is equal to the mean of its five neighbors, adjusted for the jump at the boundary. This feature is a discretized version of the mean value property of continuous harmonic functions. An interesting consequence of (19) is that the field condenses in the fractal outgrowths observed in CDT triangulations. Typically, an outgrowth is surrounded by a small boundary on which the field changes only slightly. For that reason, the field values in all simplices inside an outgrowth are almost constant. Such condensation is observed for each of the four scalar fields $\left(\overline{\phi}_i^x, \overline{\phi}_i^y, \overline{\phi}_i^z, \overline{\phi}_i^t\right)$ and in all directions, both spatial and time. Such condensations are visible as fibers in Figs. 8, 9, 10, and 11, which present two-dimensional projections of the maps where each simplex i is represented by a point with coordinates $\left(\overline{\phi}_i^x, \overline{\phi}_i^y, \overline{\phi}_i^z, \overline{\phi}_i^t\right)$. Fractal outgrowths form dense clouds of points which qualitatively resemble the conformal map in Fig. 7.

这意味着对每个单纯形 i ，其场值等于它五个邻居场值的平均值，并对边界处的跳跃做了修正。这个性质是连续调和函数平均值性质的离散版本。式 (19) 的一个有趣推论是，场会凝聚在 CDT 三角剖分中观测到的分形外延结构中。通常，外延结构被小边界包围，边界上的场变化很小。因此，外延结构内部所有单纯形的场值几乎是常数。这种凝聚现象在四个标量场 $\left(\overline{\phi}_i^x, \overline{\phi}_i^y, \overline{\phi}_i^z, \overline{\phi}_i^t\right)$ 的每个场、所有空间和时间方向上都能观测到。这种凝聚在图 8、9、10、11 中呈现为纤维状，这些图是映射的二维投影，其中每个单纯形 i 由一个坐标为 $\left(\overline{\phi}_i^x, \overline{\phi}_i^y, \overline{\phi}_i^z, \overline{\phi}_i^t\right)$ 的点表示。分形外延结构形成密集的点云，定性上与图 7 的共形映射相似。

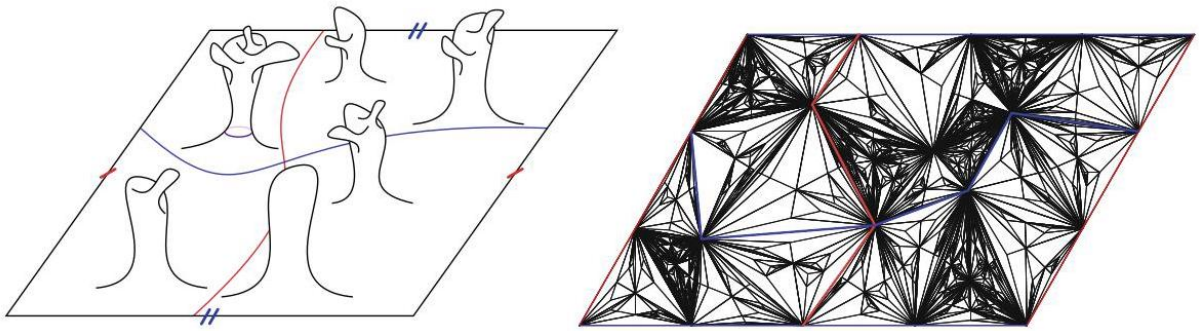

Fig. 7 Left: A two-dimensional visualization of a fractal structure of a quantum manifold with sizable outgrowths originating from the toroidal center. The boundaries of the rectangular cell are pairwise identified, making it a topological torus. Right: A visualization of a two-dimensional toroidal triangulation with

outgrowths. In CDT all triangles are assumed to be identical, but a triangulation can be transformed by a conformal map to the regular square lattice with nonidentical triangles. The quantum outgrowths are represented by denser regions

图 7 左: 量子流形分形结构的二维可视化，该流形存在源自环面中心的大量外延结构。矩形单元的边界成对认同，使其成为拓扑环面。右: 带有外延结构的二维环面三角剖分的可视化。在 CDT 中，所有三角形都假设是全等的，但可以通过共形映射将三角剖分变换为三角形不全等的正则正方格子。量子外延结构由密度更高的区域表示

Boundary redefinition The reason the scalar field is chosen to take values on S^1 with a winding number equal to one or, equivalently, introducing a jump $\delta = 1$ in the field value at a boundary, is to stretch the field values over a range $[0, 1)$. Surprisingly, the solution $\overline{\phi}_i$ given by (18) does not need to be constant on the hypersurface with the jump nor does it necessarily take values in the range $[0, 1)$ (as illustrated in Fig. 6), even after adjusting the global constant. The action of the scalar field with a jump at the boundary (15) is invariant under a simultaneous local shift of the boundary and a corresponding redefinition of the field values. The scalar field viewed as taking values on S^1 is not altered if we flip a simplex i from one side of the boundary to the other side and at the same time transform the value of the scalar field $\phi_i \to \phi_i \pm 1$, where the sign depends on whether the simplex is moved from the negative side to the positive side of the oriented boundary or vice versa. Therefore, it is always possible to continuously deform the boundary and preserve its nature as a hypersurface with the topology of T^3 , so that the classical solution $\overline{\phi}_i$ takes values in the range $[0, 1)$. A two-dimensional example of this transformation is presented in Fig. 6. For a detailed description of this procedure, we refer the reader to [21].

边界重定义选择标量场在 S^1 上取值且绕数为 1，或者等价地说，在边界处引入场值的跳变 $\delta = 1$ ，其目的是将场值拓展至整个区间 $[0, 1)$ 。令人惊讶的是，式 (18) 给出的解 $\overline{\phi}_i$ 既不需要在带有跳变的超曲面上取常数，即便调整全局常数后，也不一定在区间 $[0, 1)$ 内取值 (如图 6 所示)。在边界处带有跳变的标量场的作用量 (式 15)，在边界同时局域平移与对应场值重定义下是不变的。如果我们将单纯形 i 从边界的一侧翻转到另一侧，同时变换标量场 $\phi_i \to \phi_i \pm 1$ 的取值 (符号由单纯形是从定向边界的负侧移到正侧还是相反方向决定)，那么取值在 S^1 上的标量场本身不会发生改变。因此，我们总可以连续形变边界，同时保持它作为拓扑为 T^3 的超曲面的性质，从而让经典解 $\overline{\phi}_i$ 的取值落在区间 $[0, 1)$ 内。图 6 给出了该变换的二维示例。关于该步骤的详细描述，读者可参阅文献 [21]。

We have now achieved our goal of finding harmonic coordinates on a triangulation $\mathcal{T}$ via classical scalar fields, which are harmonic maps from the triangulation $\mathcal{T}$ to S^1 with winding number one.

我们现在已经达成了目标: 通过经典标量场在三角剖分 $\mathcal{T}$ 上得到调和坐标，这些标量场是从三角剖分 $\mathcal{T}$ 到 S^1 的绕数为 1 的调和映射。

Density Maps in Harmonic Coordinates

调和坐标中的密度图

To summarize the previous section, for a given toroidal triangulation $\mathcal{T}$, we have defined four independent non-contractible boundaries, labeled with $\mu = x, y, z, t$, in such a way that the corresponding classical solution $\overline{\phi}_i^{\mu}$ (18) to the Laplace equation with a jump at the boundary (17) interpolates from 0 on one side to 1

on the other side of the boundary. Each four-simplex i in a triangulation $\mathcal{T}$ is assigned a set of four coordinates $\left(\overline{\phi}_i^x, \overline{\phi}_i^y, \overline{\phi}_i^z, \overline{\phi}_i^t\right)$. Thus, we have managed to introduce the coordinate system:

总结上一节内容，对于给定的环面三角剖分 $\mathcal{T}$，我们定义了四个独立的不可收缩边界，标记为 $\mu = x, y, z, t$，由此得到边界 (17) 处带跳跃的拉普拉斯方程对应的经典解 $\overline{\phi}_i^\mu$ (18)，该解在边界一侧插值为 0，另一侧插值为 1。三角剖分 $\mathcal{T}$ 中的每个四单形 i 都被赋予一组四个坐标 $\left(\overline{\phi}_i^x, \overline{\phi}_i^y, \overline{\phi}_i^z, \overline{\phi}_i^t\right)$。由此我们成功引入了如下坐标系:

$$\overline{\phi}^\mu = \left(\overline{\phi}^x, \overline{\phi}^y, \overline{\phi}^z, \overline{\phi}^t\right) \in [0,1)^4.$$

The coordinates should be treated as living on a four-torus with circumference 1 in each direction, which is achieved by identifying $\overline{\phi}^\mu = 0$ and $\overline{\phi}^\mu = 1$. The scalar fields $\overline{\phi}_i^\mu$ provide harmonic maps $\overline{\phi}^\mu : \mathcal{T} \to S^1$ and serve as harmonic coordinates.

该坐标可视为定义在每个方向周长均为 1 的四维环面上，这是通过等同 $\overline{\phi}^\mu = 0$ 与 $\overline{\phi}^\mu = 1$ 实现的。标量场 $\overline{\phi}_i^\mu$ 给出调和映射 $\overline{\phi}^\mu : \mathcal{T} \to S^1$，并作为调和坐标使用。

In this section, we present the results of scalar field measurements for generic triangulations observed in all the four phases, C, C_b, B, and A of CDT with the toroidal spatial topology and time-periodic boundary conditions. The results were obtained for one typical configuration in each phase with time extent $T = 20$ and four-volume $N_{41} \approx 720\text{k}$. For each direction $\mu = x, y, z, t$, the boundary μ is aligned in such a way that the classical scalar field $\overline{\phi}^\mu \in [0,1)$ and the maximal density of points is roughly centered around $\overline{\phi}^\mu \approx 0.5$ (for visual reasons). Given a coordinate system $\overline{\phi}$, we can define volume density $\sqrt{g\left(\overline{\phi}\right)}$ as

本节我们给出具有环面空间拓扑和时间周期边界条件的 CDT 四个相 C, C_b, B 和 A 中，一般三角剖分的标量场测量结果。结果是对每个相中时间范围为 $T = 20$、四体积为 $N_{41} \approx 720\text{k}$ 的一个典型构型得到的。对于每个方向 $\mu = x, y, z, t$，边界 μ 的对齐方式使得经典标量场 $\overline{\phi}^\mu \in [0,1)$ 和点的最大密度大致中心在 $\overline{\phi}^\mu \approx 0.5$ 附近 (出于可视化考虑)。给定坐标系 $\overline{\phi}$，我们可以将体积密度 $\sqrt{g\left(\overline{\phi}\right)}$ 定义为

$$\Delta V\left(\overline{\phi}\right) = \sqrt{g\left(\overline{\phi}\right)} \prod_\mu \Delta\overline{\phi}^\mu, \tag{20}$$

which measures the number of four-simplices, which hold the four-volume, in a small region $\left[\overline{\phi}^\mu, \overline{\phi}^\mu + \Delta\overline{\phi}^\mu\right), \mu = x, y, z, t$. The density distribution $\sqrt{g\left(\overline{\phi}_i\right)}$, provided by a density plot of $\left(\overline{\phi}_i^x, \overline{\phi}_i^y, \overline{\phi}_i^z, \overline{\phi}_i^t\right)$, depends on four fields and is difficult to visualize. Therefore, in Figs. 8, 9, 10, and 11, we present two-dimensional projections (in various directions) of the density distribution, where each dot represents a simplex with coordinates determined by the classical scalar field solution $\left(\overline{\phi}_i^x, \overline{\phi}_i^y, \overline{\phi}_i^z, \overline{\phi}_i^t\right)$ [18]. In a small area $\Delta A_{\mu\nu} = \Delta\overline{\phi}^\mu \Delta\overline{\phi}^\nu$, we count the total number of four-simplices i with coordinates $\overline{\phi}_i^\sigma \in \left[\overline{\phi}_i^\sigma, \overline{\phi}_i^\sigma + \Delta\overline{\phi}^\sigma\right), \sigma = \mu, \upsilon$; other directions are projected on the $\left(\overline{\phi}^\mu, \overline{\phi}^\upsilon\right)$-plane.

它用来测量小区域 $\left[\overline{\phi}^{\mu}, \overline{\phi}^{\mu} + \Delta\overline{\phi}^{\mu}\right), \mu = x, y, z, t$ 中承载四体积的四单形数量。由 $\left(\overline{\phi}_i^x, \overline{\phi}_i^y, \overline{\phi}_i^z, \overline{\phi}_i^t\right)$ 的密度图得到的密度分布 $\sqrt{g\left(\overline{\phi}_i\right)}$ 依赖于四个场，难以可视化。因此在图 8、9、10、11 中，我们给出密度分布的 (不同方向的) 二维投影，其中每个点代表一个坐标由经典标量场解 $\left(\overline{\phi}_i^x, \overline{\phi}_i^y, \overline{\phi}_i^z, \overline{\phi}_i^t\right)$ [18] 确定的单形。我们对小区域 $\Delta A_{\mu\nu} = \Delta\overline{\phi}^{\mu}\Delta\overline{\phi}^{\nu}$ 中坐标为 $\overline{\phi}_i^{\sigma} \in \left[\overline{\phi}_i^{\sigma}, \overline{\phi}_i^{\sigma} + \Delta\overline{\phi}^{\sigma}\right), \sigma = \mu, \upsilon$ 的四单形 i 总数进行计数，其他方向投影到 $\left(\overline{\phi}^{\mu}, \overline{\phi}^{\upsilon}\right)$ 平面上。

The two-dimensional projections of the density distribution for a configuration in the semiclassical phase $C(\kappa_0 = 4.0, \Delta = 0.2, T = 20)$ are presented in Fig. 8. The color of each point depends on the original time coordinate t that enumerates the leaves of the proper-time foliation. Simplices belonging to a slab between slices $t \in \mathbb{N}$ and $t+1$ are assigned a non-integer time coordinate: $t, t+\frac{1}{4}, t+\frac{1}{2}$ and $t+\frac{3}{4}$ to the $(4,1)-, (3,2)-, (2,3)-$, and $(1,4)-$ simplices, respectively. In total, the non-integer time coordinate can take one of the $4 \times T$ values. The graph on the left-hand side in Fig. 8 is a projection on the $\overline{\phi}^t - \overline{\phi}^x$ plane, while the graph on the right-hand side is a projection on the $\overline{\phi}^x - \overline{\phi}^y$ plane. The apparent correspondence between the color of points (t -coordinate) and the horizontal axis ($\overline{\phi}^t$ -coordinate) observed in the left graph expresses a strong correlation of the scalar field having a jump in the time direction with the original time slicing. The large-scale structure observed in the right graph $\left(\overline{\phi}^x - \overline{\phi}^y\right.$ projection) is quite isotropic and homogeneous in all spatial directions, i.e., it looks qualitatively the same for all $\overline{\phi}^x - \overline{\phi}^y, \overline{\phi}^x - \overline{\phi}^z$ and $\overline{\phi}^y - \overline{\phi}^z$ projections and also when shifted or rotated. However, on smaller scales, this large-scale homogeneity and isotropy is broken. Sparse regions represent the central toroidal part, and dense regions show fractal outgrowths, which are nontrivially correlated and form the characteristic cosmic voids and (it is a structure of cosmic voids and fibers) structure.

我们在图 8 中展示了半经典相位 $C(\kappa_0 = 4.0, \Delta = 0.2, T = 20)$ 下某构型密度分布的二维投影。每个点的颜色由原时间坐标 t 决定，该坐标用于枚举固有时叶状结构的叶片。位于切片 $t \in \mathbb{N}$ 与 $t+1$ 之间 slab 内的单形被赋予非整数时间坐标: 分别对 $(4,1)-, (3,2)-, (2,3)-$ 单形、$(1,4)-$ 单形赋予 $t, t+\frac{1}{4}, t+\frac{1}{2}$ 和 $t+\frac{3}{4}$。非整数时间坐标总共有 $4 \times T$ 种可能取值。图 8 左图是投影到 $\overline{\phi}^t - \overline{\phi}^x$ 平面的结果，右图是投影到 $\overline{\phi}^x - \overline{\phi}^y$ 平面的结果。左图中可观测到点的颜色 (t 坐标) 与横轴 ($\overline{\phi}^t$ 坐标) 存在明显对应，说明沿时间方向存在跳变的标量场与原始时间切片具有强相关性。右图 $\left(\overline{\phi}^x - \overline{\phi}^y\right.$ 投影中观测到的大尺度结构在所有空间方向上都相当各向同性且均匀，即所有 $\overline{\phi}^x - \overline{\phi}^y, \overline{\phi}^x - \overline{\phi}^z$ 和 $\overline{\phi}^y - \overline{\phi}^z$ 投影、以及平移或旋转后的结果，定性看起来都是一致的。然而在更小尺度上，这种大尺度的均匀性与各向同性被打破。稀疏区域对应环面中心部分，致密区域呈现分形生长，它们之间存在非平庸关联，形成了典型的宇宙空洞与纤维结构。

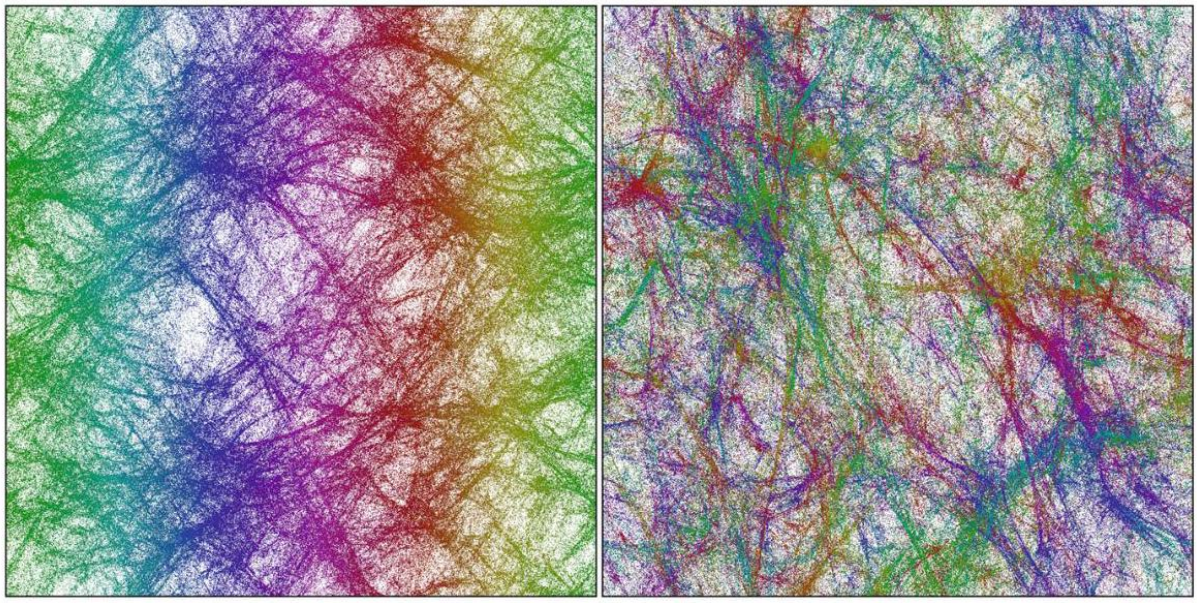

Fig. 8 Cosmic voids and filaments for a configuration in phase C ($\kappa_0 = 3.0, \Delta = 0.2, T = 20$) . The charts present projections of the volume density maps on the $\overline{\phi}^t - \overline{\phi}^x$ plane (left) and on the $\overline{\phi}^x - \overline{\phi}^y$ plane (right)

图 8 相位 C ($\kappa_0 = 3.0, \Delta = 0.2, T = 20$) 下某构型的宇宙空洞与纤维。本图展示了体积密度图在 $\overline{\phi}^t - \overline{\phi}^x$ 平面 (左) 和 $\overline{\phi}^x - \overline{\phi}^y$ 平面 (右) 的投影

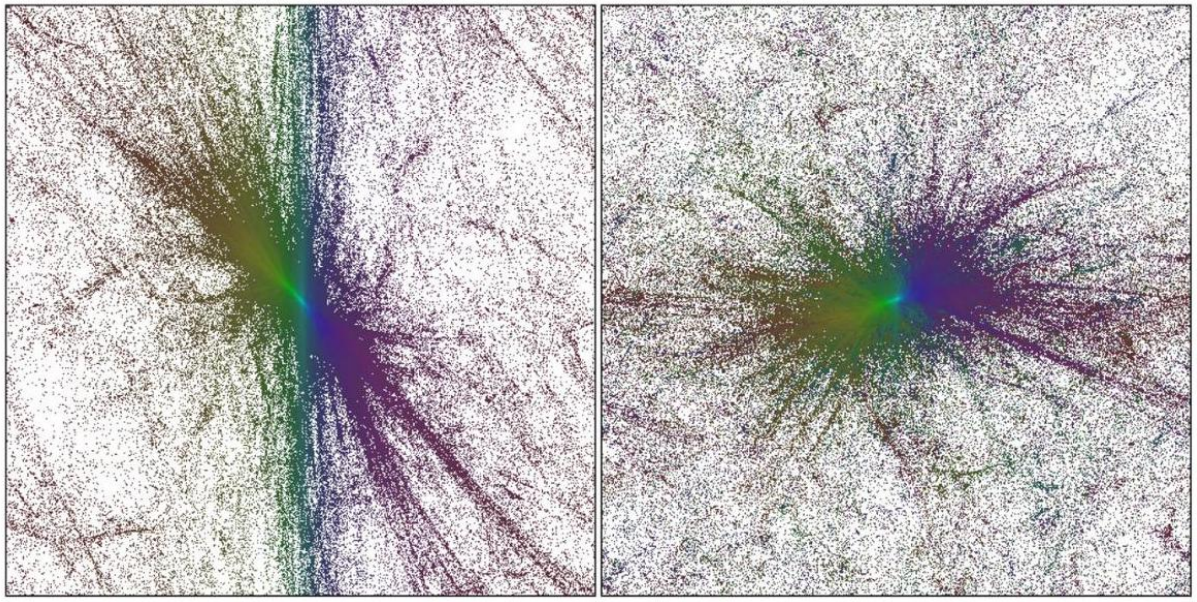

Fig. 9 A configuration in phase C_b with $T = 20$ ($\kappa_0 = 2.5, \Delta = 0.2$) . The charts present projections of the volume density maps on the $\overline{\phi}^t - \overline{\phi}^x$ plane (left) and on the $\overline{\phi}^x - \overline{\phi}^y$ plane (right)

图 9 相位 C_b 下带有 $T = 20$ ($\kappa_0 = 2.5, \Delta = 0.2$) 的构型。本图展示了体积密度图在 $\overline{\phi}^t - \overline{\phi}^x$ 平面 (左) 和 $\overline{\phi}^x - \overline{\phi}^y$ 平面 (右) 的投影

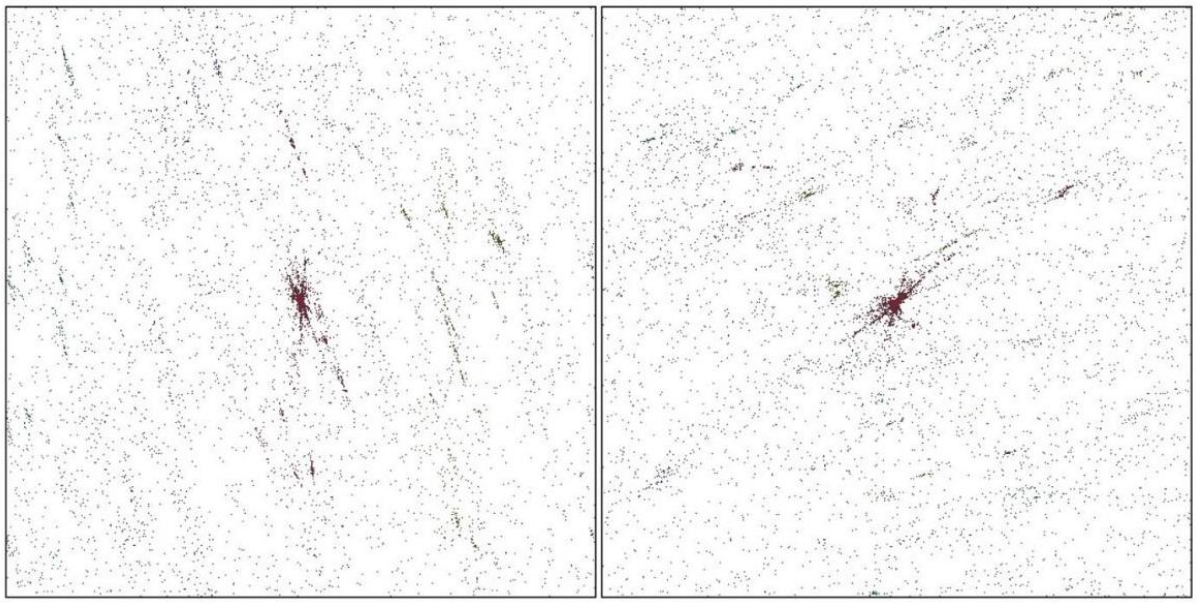

Fig. 10 A configuration in phase B with $T = 4\,(\kappa_0 = 4.4, \Delta = -0.7)$. The charts present projections of the volume density maps on the $\overline{\phi}^t - \overline{\phi}^x$ plane (left) and on the $\overline{\phi}^x - \overline{\phi}^y$ plane (right)

图 10 相位 B 下带有 $T = 4\,(\kappa_0 = 4.4, \Delta = -0.7)$ 的构型。本图展示了体积密度图在 $\overline{\phi}^t - \overline{\phi}^x$ 平面 (左) 和 $\overline{\phi}^x - \overline{\phi}^y$ 平面 (右) 的投影

Interestingly, although we are analyzing the case of pure gravity without a backreaction of classical scalar fields on quantum geometries, and the measured universes are only a few Planck lengths in diameter, they qualitatively reproduce the basic features of the real Universe, including the large-scale cosmic voids and filaments structure observed in nature. From this perspective, it is conceivable that geometric fractal outgrowths serve as seeds for certain condensations of the matter field (this is indeed the case for quantum scalar fields coupled to geometry, discussed in the next section), leading to the creation of nontrivial structures resulting from quantum gravity.

有趣的是，尽管我们分析的是纯引力情形，未考虑经典标量场对量子几何的反作用，且测得的宇宙直径仅为几个普朗克长度，但它们在定性上复现了真实宇宙的基本特征，包括自然界中观测到的大尺度宇宙空洞与纤维结构。从该视角来看，几何分形生长完全可以成为物质场某些凝聚过程的种子 (对于耦合几何的量子标量场情况确实如此，我们将在下一节讨论)，进而由量子引力作用产生非平庸结构。

A similar analysis can also be performed for typical triangulations that appear in other CDT phases. In Fig. 9, we plot two-dimensional projections of the density maps measured in the bifurcation phase C_b for $T = 20$. As before, the geometry appears fairly isotropic in all directions, but is no longer homogeneous. The lack of homogeneity in the time direction is well explained by the nonuniform spatial-volume distribution in the proper-time coordinate t since the volume profile visible for large T in phase C_b is bell-shaped in contrast to flat in the C phase. A characteristic feature of general triangulations of the C_b phase is the formation of dense clusters of volumes around high-order vertices observed in every second spatial slice, which makes the spatial-volume distribution inhomogeneous in spatial directions as well. The maps presented in Fig. 9 for

phase C_b , unlike phase C , miss the nontrivial structure of fractal outgrowths, as the geometry viewed from any direction appears to concentrate in only one large outgrowth.

类似分析也可应用于出现在其他 CDT 相中的典型三角剖分。在图 9 中，我们绘制了分岔相 C_b 中针对 $T = 20$ 测得的密度图的二维投影。和之前一样，几何在所有方向上都表现出相当好的各向同性，但不再均匀。时间方向上的非均匀性可以用固有时间坐标 t 中的非均匀空间体积分布很好地解释: 对于大 T ，相 C_b 中可见的体积轮廓呈钟形，而 C 相中的体积轮廓是平坦的。C_b 相的一般三角剖分的一个特征是，每隔一个空间切片就会在高阶顶点周围形成致密的体积团，这也使得空间方向上的体积分布同样变得非均匀。图 9 中给出的 C_b 相的密度图，和 C 相不同，缺失了分形生长的非平庸结构，因为从任意方向观测，几何都只集中在一个大生长区域中。

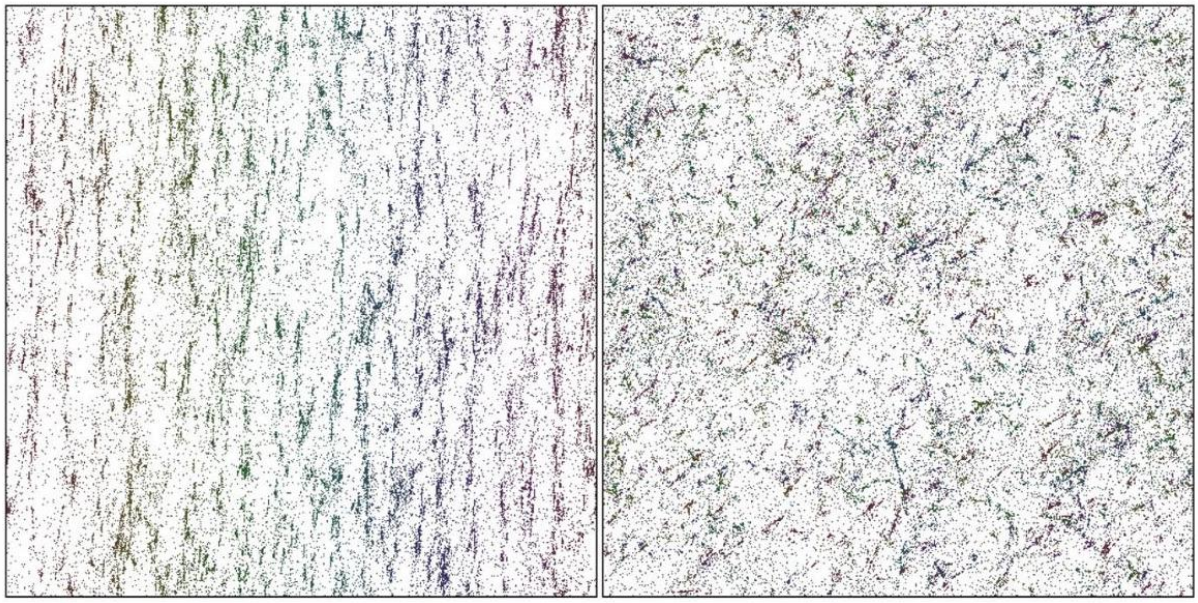

Fig. 11 A configuration in phase A with $T = 20\,(\kappa_0 = 5.0, \Delta = 0.2)$. The charts present projections of the volume density maps on the $\overline{\phi}^t - \overline{\phi}^x$ plane (left) and on the $\overline{\phi}^x - \overline{\phi}^y$ plane (right)

图 11 A 相中带有 $T = 20\,(\kappa_0 = 5.0, \Delta = 0.2)$ 的一个构型。图中分别给出了体积密度图在 $\overline{\phi}^t - \overline{\phi}^x$ 平面 (左) 和 $\overline{\phi}^x - \overline{\phi}^y$ 平面 (右) 上的投影

This effect is even more pronounced in the B phase; see Fig. 10 showing the configuration with $T = 4$. In this case, the geometry in all directions effectively becomes compactified to a point. Thus, both temporal and spatial homogeneities are maximally broken. This was expected from previous analyses of the geometric configurations observed in this phase. Finally, Fig. 11 shows a typical configuration of phase A with $T = 20$. In this case, the dense regions corresponding to geometric outgrowths are separated and uncorrelated and do not form any nontrivial structures. This kind of behavior was observed earlier in the time direction, but now appears also in spatial directions. Consequently, the overall configuration measured in the A phase is highly homogeneous and isotropic on both the large and small scales.

这种效应在 B 相中更为显著；参见图 10，它展示了带有 $T = 4$ 的构型。在该情形下，所有方向的几何实际上都紧致化为一个点。因此，时间均匀性和空间均匀性都被最大程度破坏了，这和此前对该相中几何构型的分析得到的预期一致。最后，图 11 展示了 A 相中带有 $T = 20$ 的一个典型构型。在该情形下，对应几何生长的致密区域相互分离、互不关联，不形成任何非平庸结构。这类行为此前仅在时间方向观测到，现在也在空间方向出现。因此，在 A 相中测得的整体构型在大尺度和小尺度上都高度均匀且各向同性。

Dynamical Scalar Fields

动力学标量场

In this section we will introduce dynamical scalar fields in the four-dimensional model of Causal Dynamical Triangulations and study their backreaction on the underlying quantum geometries. Such a field, minimally coupled to quantum gravity, presents a simple example of quantum matter which can be added to CDT. Here, we review recent studies for toroidal spatial topology (see section "Classical Scalar Fields"), but models of this type for spherical spatial topology were also studied in EDT and CDT [22-25].

本节我们将在因果动态三角剖分的四维模型中引入动力学标量场，研究它们对基础量子几何的反作用。这种与量子引力最小耦合的场是可添加到 CDT 中的简单量子物质实例。在此我们综述环面空间拓扑的最新研究 (参见“经典标量场”小节)，这类空间拓扑为球面的模型也已在 EDT 和 CDT 中得到研究 [22-25]。

The lattice regularization of the continuous massless scalar field action (5) is given by

连续无质量标量场作用量 (5) 的格点正则化由下式给出

$$S_M[\phi, \mathcal{T}] = \frac{1}{2} \sum_{i \leftrightarrow j} (\phi_i - \phi_j)^2 = \sum_{i,j} \phi_i L_{ij} \phi_j, \tag{21}$$

where, as before, the discrete Laplacian $\mathbf{L}$ is given by (10). The value of the dynamical scalar field ϕ_i is located in the center of the simplex i . The lattice-regularized path integral of quantum gravity (3) including an integral over scalar fields ϕ reads:

和之前一样，其中离散拉普拉斯算子 $\mathbf{L}$ 由式 (10) 给出。动力学标量场 ϕ_i 的值定义在单纯形 i 的中心。包含标量场 ϕ 积分的量子引力 (3) 的格点正则化路径积分如下:

$$\mathcal{Z}_{\mathrm{CDT}} = \sum_{\mathcal{T}} \int \mathcal{D}[\phi] \, \mathrm{e}^{-(S_R[\mathcal{T}] + S_M[\phi, \mathcal{T}])}. \tag{22}$$

In (22) a flat measure over fields was used:

式 (22) 中采用了场的平测度:

$$\mathcal{D}[\phi] = \prod_i{}' \frac{\mathrm{d}\phi_i}{\sqrt{\pi}}, \tag{23}$$

where the prime index indicates elimination of integration over the constant zero-mode of the Laplacian L. Due to the Gaussian form of the field in the partition function (22), for a given triangulation $\mathcal{T}$, the fields can be integrated out leading to a quantum correction:

式中撇号标记表示去掉拉普拉斯 L 常数零模的积分。由于配分函数 (22) 中场是高斯型的，对于给定三角剖分 $\mathcal{T}$ ，可对场积分得到量子修正:

$$S^{\text{eff}}_{\text{quant}}\left[\mathcal{T}\right] = \frac{1}{2}\log\det\left(\mathbf{L}'\left[\mathcal{T}\right]\right) \tag{24}$$

to the geometric action $S_R\left[\mathcal{T}\right] \to S_R\left[\mathcal{T}\right] + S^{\text{eff}}_{\text{quant}}\left[\mathcal{T}\right]$. The matrix $\mathbf{L}'$ is the Laplacian matrix $\mathbf{L}$ in the subspace orthogonal to the zero mode of $\mathbf{L}$ and depends on the geometry through the adjacency matrix $\mathbf{A}$ defined for a given triangulation $\mathcal{T}$. Such a dynamical field ϕ can be rescaled $\phi \to \lambda\phi$; however, this rescaling can be absorbed by a redefinition of the cosmological constant and the measure.

这是对几何作用量 $S_R\left[\mathcal{T}\right] \to S_R\left[\mathcal{T}\right] + S^{\text{eff}}_{\text{quant}}\left[\mathcal{T}\right]$ 的修正。矩阵 $\mathbf{L}'$ 是拉普拉斯矩阵 $\mathbf{L}$ 在正交于 $\mathbf{L}$ 零模的子空间中的部分，它通过给定三角剖分 $\mathcal{T}$ 定义的邻接矩阵 $\mathbf{A}$ 依赖于几何。这类动力学场 ϕ 可以做重新标度 $\phi \to \lambda\phi$ ； 不过这种重新标度可以被宇宙学常数和测度的重新定义吸收。

The main conclusion to be drawn from the earlier results [22] is that the backreaction of the massless scalar field(s) on the geometry is negligible and mainly leads to a slight shift of the coupling constants. Adding a potential term, for example, a mass term only dampens field fluctuations and does not alter the geometric phase structure. Similarly, increasing the number of scalar fields did not affect the phase structure. This suggests that the determinant $S^{\text{eff}}_{\text{quant}}\left[\mathcal{T}\right]$ is weakly dependent on $\mathcal{T}$ and its impact can be neglected.

从早期结果 [22] 得到的主要结论是，无质量标量场对几何的反作用可以忽略，仅会导致耦合常数发生微小偏移。添加势能项 (例如质量项) 只会抑制场涨落，不会改变几何相结构。同理，增加标量场数目也不会影响相结构。这说明行列式 $S^{\text{eff}}_{\text{quant}}\left[\mathcal{T}\right]$ 对 $\mathcal{T}$ 的依赖很弱，其影响可以忽略。

Target topology and jumps In section ”Classical Scalar Fields,” a coordinate system was defined using classical scalar fields taking values on a manifold with the topology matching that of the underlying spacetime manifold. Since the topology of the target space turned out to be crucial in a meaningful definition of the coordinate system, it is tempting to consider dynamical scalar fields with the same target topology, that is, of a torus. Such studies were carried out in [26].

目标拓扑与跃变在“经典标量场”小节中，我们利用经典标量场定义了坐标系，这些场在流形上的取值与基础时空流形具有相同拓扑。由于目标空间拓扑对定义有意义的坐标系至关重要，我们很自然会考虑具有相同目标拓扑 (即环面拓扑) 的动力学标量场。这类研究已在文献 [26] 中完成。

The spatial topology is chosen as the three-torus T^3 , and, since periodic time conditions are assumed, the topology of the spacetime manifold is the four-torus T^4 . The dynamical scalar field now takes values in a circle of circumference δ and is forced to wind once around the circle when moving around a non-contractible loop in one of the directions on T^4 . As explained in the previous section, such a field can be viewed as taking values in $\mathbb{R}$ with a jump of magnitude δ when crossing the unphysical boundary. It should be noted that in the case of dynamical scalar fields, the size of the jump δ is relevant, and thus it is explicitly reintroduced in this section.

我们将空间拓扑取为三维环面 T^3，又由于假设了周期性时间条件，因此时空流形的拓扑为四维环面 T^4。此时动力学标量场的取值位于周长为 δ 的圆周上，当沿 T^4 某一方向的不可收缩环运动一周时，标量场必定绕圆周缠绕一次。如前一小节所述，这种场可以看作取值在 $\mathbb{R}$ 中，穿过非物理边界时会产生大小为 δ 的跃变。需要注意的是，对于动力学标量场，跃变的大小 δ 是相关量，因此本节明确引入了它。

Enforcing nontrivial winding numbers for scalar fields impacts the dynamics of the geometry-matter interaction. For the $\mathbb{R}$ -valued scalar field without a jump, i.e., with a zero winding number, the classical solution becomes a constant field configuration which is the absolute minimum (zero) of the matter action.

对标量场施加非平凡缠绕数会影响几何-物质相互作用的动力学。对于没有跃变 (即缠绕数为零) 的 $\mathbb{R}$ 值标量场，经典解是常数场构型，这是物质作用量的绝对最小值 (零)。

The action Let us consider the full quantum action of a massless scalar field with a single winding number on a circle S^1 of circumference δ :

作用量我们考虑周长为 δ 的圆周 S^1 上具有单个缠绕数的无质量标量场的完全量子作用量:

$$S_M[\phi, \delta, \mathcal{T}] = \frac{1}{2}\sum_{i\leftrightarrow j}\left(\phi_i - \phi_j - \delta B_{ij}\right)^2 = \sum_{i,j}\phi_i L_{ij}\phi_j - 2\delta\sum_i \phi_i b_i + \delta^2 \cdot V. \tag{25}$$

As before, $B_{ij} = +1/-1$ when the boundary face $i \to j$ is crossed in the positive/negative direction and is zero otherwise. The jump vector $b_i = \sum_j B_{ij}$ and the boundary volume $V = \frac{1}{2}\sum_{i,j} B_{ij}^2$. The magnitude of the jump δ sets the scale of the field ϕ . Again, the field ϕ can be integrated out because the action (25) is still Gaussian but with an additional linear term, which can be eliminated by a shift of the field ϕ . We decompose the field into the classical part $\overline{\phi}$ and the quantum part ξ :

与前述一致，$B_{ij} = +1/-1$ 当沿正方向/负方向穿过边界面 $i \to j$ 时取值为该值，否则为零。跃变矢量为 $b_i = \sum_j B_{ij}$，边界体积为 $V = \frac{1}{2}\sum_{i,j} B_{ij}^2$。跃变的幅度 δ 设定了场 ϕ 的标度。同理，由于作用量 (25) 仍为高斯型，场 ϕ 可被积出，仅多一个线性项，可通过场 ϕ 的平移消去该项。我们将场分解为经典部分 $\overline{\phi}$ 和量子部分 ξ :

$$\phi_i = \overline{\phi}_i + \xi_i, \tag{26}$$

where both ϕ_i and $\overline{\phi}_i$ have winding number one. Therefore, the fluctuation field ξ is a scalar field with a winding number 0, like an ordinary scalar field that takes values in $\mathbb{R}$. The classical field $\overline{\phi}$ minimizes the action (25) and satisfies the equation:

其中 ϕ_i 和 $\overline{\phi}_i$ 的绕数均为 1。因此，涨落场 ξ 是绕数为 0 的标量场，就像取值于 $\mathbb{R}$ 的普通标量场。经典场 $\overline{\phi}$ 使作用量 (25) 取极小值，满足方程:

$$\mathbf{L}\overline{\phi} = \delta \cdot b,\ \overline{\phi} = \delta \cdot \mathbf{L}'^{-1} b, \tag{27}$$

where $\mathbf{L}'$ is the discrete Laplacian matrix $\mathbf{L}$ with a modification that ensures that $\overline{\phi}_{i_1} = 0$, as in (18), and which makes $\mathbf{L}'$ invertible. The action (25) can be split into the classical part S_{class} and the quantum part S_{quant} :

其中 $\mathbf{L}'$ 是经修正的离散拉普拉斯矩阵 $\mathbf{L}$ ， 该修正保证了如 (18) 式的 $\overline{\phi}_{i_1} = 0$ ， 并使 $\mathbf{L}'$ 可逆。作用量 (25) 可拆分为经典部分 S_{class} 和量子部分 S_{quant} ：

$$S_M\left[\phi = \overline{\phi} + \xi, \delta, \mathcal{T}\right] = S_{\text{class}}\left[\delta, \mathcal{T}\right] + S_{\text{quant}}\left[\xi, \mathcal{T}\right]$$

$$S_{\text{class}}\left[\delta, \mathcal{T}\right] = \sum_{i,j} \overline{\phi}_i L_{ij} \overline{\phi}_j - 2\delta \sum_i \overline{\phi}_i b_i + \delta^2 \cdot V$$

$$S_{\text{quant}}\left[\xi, \mathcal{T}\right] = \sum_{i,j} \xi_i L_{ij} \xi_j \tag{28}$$

The classical solution $\overline{\phi}$ is fully determined by triangulation $\mathcal{T}$, together with the nonphysical boundary, through (27) and is proportional to the jump size δ . Therefore, the classical contribution $S_{\text{class}}\left[\mathcal{T}, \delta\right]$ depends effectively only on triangulation $\mathcal{T}$ and is quadratic in δ .

经典解 $\overline{\phi}$ 由三角剖分 $\mathcal{T}$ 连同非物理边界通过 (27) 式完全确定，且与跃变大小 δ 成正比。因此，经典贡献 $S_{\text{class}}\left[\mathcal{T}, \delta\right]$ 实际上仅依赖于三角剖分 $\mathcal{T}$ ， 且是 δ 的二次型。

After integrating out the quantum fluctuations ξ of the field using the modified integration measure, $\mathcal{D}\left[\phi\right] = \mathcal{D}\left[\xi\right]$, the field contribution to the geometric action is given by

采用修正积分测度 $\mathcal{D}\left[\phi\right] = \mathcal{D}\left[\xi\right]$ 积出场的量子涨落 ξ 后，场对几何作用量的贡献由下式给出:

$$S^{\text{eff}}\left[\delta, \mathcal{T}\right] = S^{\text{eff}}_{\text{quant}}\left[\mathcal{T}\right] + S_{\text{class}}\left[\delta, \mathcal{T}\right].$$

The effective quantum correction $S^{\text{eff}}_{\text{quant}}\left[\mathcal{T}\right]$ comes from integrating out Gaussian field fluctuations ξ described by the quantum part $S_{\text{quant}}\left[\xi, \mathcal{T}\right]$ and given by a logarithm of the determinant of $\mathbf{L}'$ (24) . The additional correction term $S_{\text{class}}\left[\delta, \mathcal{T}\right]$ is the scalar field action (25) calculated for the classical solution $\overline{\phi}$ that satisfies (27)

有效量子修正 $S^{\text{eff}}_{\text{quant}}\left[\mathcal{T}\right]$ 来自积出由量子部分 $S_{\text{quant}}\left[\xi, \mathcal{T}\right]$ 描述的高斯场涨落 ξ ， 其形式为 $\mathbf{L}'$ (24) 的行列式的对数。额外修正项 $S_{\text{class}}\left[\delta, \mathcal{T}\right]$ 是满足 (27) 式的经典解 $\overline{\phi}$ 对应的标量场作用量 (25)

$$S_{\text{class}}\left[\delta, \mathcal{T}\right] = -\delta \sum_i \overline{\phi}_i b_i + \delta^2 \cdot V = -\delta^2 \sum_{i,j} \left(b_i L'^{-1}_{ij} b_j - \frac{B^2_{ij}}{2} \right)$$

$$= -\frac{1}{2} \sum_{i,j} \delta B_{ij} \left(\overline{\phi}_i - \overline{\phi}_j - \delta B_{ij} \right). \tag{29}$$

Although the action (29) is, in fact, independent of the exact location of the boundary, the above equation shows that the classical action $S_{\text{class}}\left[\delta, \mathcal{T}\right]$ depends only on the values of $\overline{\phi}_i$ next to the boundary, where the jump occurs.

尽管作用量 (29) 实际上与边界的具体位置无关，但上式表明经典作用量 $S_{\text{class}}\,[\delta,\mathcal{T}]$ 仅依赖于跃变发生处边界邻近的 $\overline{\phi}_i$ 的取值。

For a given triangulation $\mathcal{T}$, the purely quantum correction from the quantum fluctuations of the scalar field $S^{\text{eff}}_{\text{quant}}\,[\mathcal{T}]$ does not depend on the jump magnitude δ and is exactly the same whether the scalar field takes values in $\mathbb{R}$ (and thus only fluctuates around 0) or in a circle S^1 of circumference δ (and fluctuates around the classical solution $\overline{\phi}_i$ with winding number one). The contribution of the classical part of the matter action $S_{\text{class}}\,[\mathcal{T},\delta]$ is quadratic in jump size δ and depends in a crucial way on triangulation $\mathcal{T}$. We expect that for a sufficiently large value of δ , it will dominate and overwhelm the geometric action (4), thus having a huge impact on the underlying quantum geometry. Indeed, such an effect is observed, as described in the next section and explained in the following section.

对于给定的三角剖分 $\mathcal{T}$ ，标量场 $S^{\text{eff}}_{\text{quant}}\,[\mathcal{T}]$ 量子涨落产生的纯量子修正不依赖于跳变幅度 δ ，且无论标量场取值于 $\mathbb{R}$ (因此仅在 0 附近涨落) 还是周长为 δ 的圆周 S^1 (绕数为 1 时在经典解 $\overline{\phi}_i$ 附近涨落)，该修正都完全相同。物质作用量 $S_{\text{class}}\,[\mathcal{T},\delta]$ 经典部分的贡献是跳变幅度 δ 的二次项，且关键依赖于三角剖分 $\mathcal{T}$ 。我们预期，当 δ 取值足够大时，该贡献将占主导并超过几何作用量 (4)，从而对底层量子几何产生巨大影响。事实上如下一节所述、后文中解释的，我们确实观测到了这种效应。

Single Scalar Field with a Jump in the Time Direction

时间方向带跃变的单个标量场

Here we present results of numerical Monte Carlo simulations obtained for one dynamical scalar field taking values in a circle S^1 of circumference δ (magnitude of the jump) with winding number one in the time direction in CDT with the toroidal spatial topology and time-periodic boundary conditions. The jump in time direction is introduced at a time boundary which is the spatial slice in layer $t = 1$ (between the periodic proper-time coordinates $t = T$ and $t = 1$), that is, at the crossing between the field values inside the $(1,4)$ -simplices in the last slab (with one vertex in $t = T$ and four vertices in $t = 1$) and the $(4,1)$ -simplices in the first slab (with four vertices in $t = 1$ and one vertex in $t = 2$). As noted earlier, the formulation is independent of the exact boundary position, and any other spatial layer or a more complicated boundary orthogonal to the time direction could be used.

我们在此呈现四维因果动态三角剖分 (CDT) 中单个动力学标量场的数值蒙特卡洛模拟结果，该标量场取值于周长为 δ (跃变幅度) 的圆 S^1 ，在环面空间拓扑与时间周期边界条件下，时间方向绕数为 1。时间方向的跃变被引入位于层 $t = 1$ (周期原时坐标 $t = T$ 与 $t = 1$ 之间) 的时间边界，即位于最后一块 slab 中 $(1,4)$ -单形 (一个顶点在 $t = T$ ，四个顶点在 $t = 1$) 和第一块 slab 中 $(4,1)$ -单形 (四个顶点在 $t = 1$ ，一个顶点在 $t = 2$) 的场值交界面处。如前文所述，该构造与边界的具体位置无关，也可选择任意其他空间层，或更复杂的正交于时间方向的边界。

The spatial three-volume n_t is defined as the number of tetrahedra in a spatial slice t , where $t = 1 \ldots T$ is the original discrete time coordinate that enumerates the leaves of the proper-time foliation. Figure 12 presents spatial volume profiles $\langle n_t \rangle$ averaged over many Monte Carlo configurations for various jump sizes, $\delta = 1, 2, 4$, and 8. MC simulations were performed inside the semiclassical phase C $(\kappa_0 = 2.2, \Delta = 0.6)$ for toroidal CDT configurations with lattice volume $N_{41} = 160\text{k}$ and the proper-time period $T = 20$. The Einstein-

Hilbert action (2), and consequently the Regge action (4), is invariant under time translations. For time-periodic boundary conditions, a direct average $\langle n_t \rangle$ would give a constant function of time t, without capturing the shape of individual configurations. In order to obtain a meaningful average volume profile $\langle n_t \rangle$, before performing the average over triangulations, the center of volume of each individual profile n_t was shifted in the (periodic) proper-time axis to the centers of the charts, $t = \frac{1}{2}T$ [21]. An identical procedure was performed for the spatial spherical topology and the de Sitter phase, where the volume profiles n_t were also bell-shaped [27]. This procedure produces an artificial slight bulge visible for small jump magnitudes ($\delta = 1, 2$). Nonetheless, a clear phase transition occurs above $\delta = 2$.

空间三体积 n_t 定义为空间切片 t 中四面体的数量，其中 $t = 1 \ldots T$ 是枚举原时分层叶的原始离散时间坐标。图 12 给出了不同跃变幅度下，对大量蒙特卡洛构型平均得到的空间体积轮廓 $\langle n_t \rangle$，$\delta = 1, 2, 4$，和 8。蒙特卡洛模拟是在半经典相 C ($\kappa_0 = 2.2, \Delta = 0.6$) 内进行的，针对格点体积为 $N_{41} = 160$k、原时周期为 $T = 20$ 的环面 CDT 构型。爱因斯坦-希尔伯特作用量 (2)，以及由此得到的雷杰作用量 (4)，都具有时间平移不变性。对于时间周期边界条件，直接对 $\langle n_t \rangle$ 求平均会得到关于时间 t 的常数函数，无法体现单个构型的轮廓形状。为了得到有意义的平均体积轮廓 $\langle n_t \rangle$，在对三角剖分求平均之前，我们将每个单独轮廓 n_t 的体积中心沿 (周期) 原时轴移到了图的中心，$t = \frac{1}{2}T$ [21]。对空间球面拓扑和德西特相也采用了相同的操作，得到的体积轮廓 n_t 同样为钟形 [27]。该操作会在小跃变幅度 ($\delta = 1, 2$) 处产生一个可见的人工微小凸起，但即便如此，在 $\delta = 2$ 以上仍会发生清晰的相变。

For small jump magnitudes ($\delta \leq 2$), one observes flat volume profiles characteristic for toroidal CDT in the pure gravity case, i.e., without scalar fields. For large magnitudes of the jump ($\delta \geq 4$), volume profiles completely change and a bell-shaped profile emerges. As shown in Fig. 12, the cosine function fits the average volume profile $\langle n_t \rangle$ very well for the largest jump size $\delta = 8$. This effect will be explained in the next section.

对于小跃变幅度 ($\delta \leq 2$)，可以观测到平直体积轮廓，这是纯引力 (即不包含标量场) 情况下环面 CDT 的特征。对于大跃变幅度 ($\delta \geq 4$)，体积轮廓发生完全改变，出现了钟形轮廓。如图 12 所示，余弦函数对最大跃变尺寸 $\delta = 8$ 对应的平均体积轮廓 $\langle n_t \rangle$ 拟合得非常好。这一效应我们会在下一节解释。

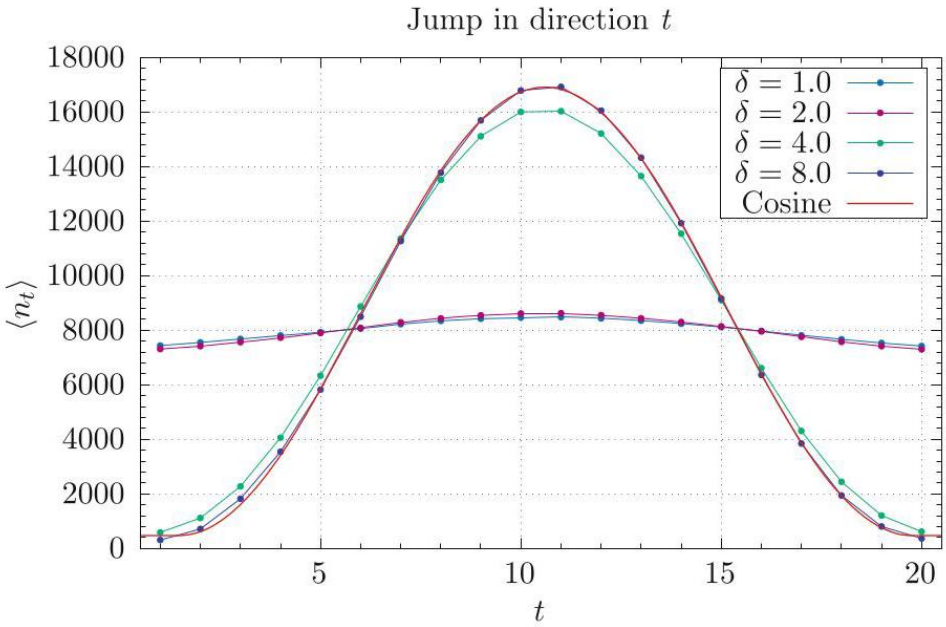

Fig. 12 Spatial volume profile n_t averaged over many MC configurations inside the semiclassical phase $C(\kappa_0 = 2.2, \Delta = 0.6)$ for $T = 20$ with scalar field jump magnitudes $\delta = 1, 2, 4, 8$. Red solid line is a fit of the function: $c + a\cos(b(t - t_0))$

图 12 半经典相 $C(\kappa_0 = 2.2, \Delta = 0.6)$ 内，对 $T = 20$ 大量蒙特卡洛构型平均得到的空间体积轮廓 n_t ，对应标量场跃变幅度 $\delta = 1, 2, 4, 8$ 。红色实线是对函数 $c + a\cos(b(t - t_0))$ 的拟合

The Minisuperspace Model

超空间模型

It can be observed that introducing a dynamical scalar field with winding number one on a circle of circumference δ enhances a pinching region, where the spatial volume of slices is small. In such a region, the field changes rapidly; nevertheless, its contribution to matter action (25) is small due to a few simplices involved.

可以观察到，在周长为 δ 的圆周上引入一个缠绕数为 1 的动力学标量场，会增强切片空间体积较小的收缩区域。在该区域中，场变化迅速；但由于涉及的单纯形数量较少，它对物质作用量 (25) 的贡献很小。

Let us consider a simplified continuous model that assumes spatial homogeneity and isotropy, where all geometrical degrees of freedom are frozen except the spatial volume $v(t) = a^3(t)$ with $a(t, x) = a(t)$ being the scale factor. Under such assumptions, the Einstein-Hilbert action (2) for the toroidal spatial topology T^3 with time-periodic boundary conditions reduces to a minisuperspace action:

我们来考虑一个假设空间均匀各向同性的简化连续模型，该模型中除空间体积 $v(t) = a^3(t)$ 外所有几何自由度都被冻结，其中 $a(t, x) = a(t)$ 是标度因子。在此假设下，具有时间周期边界条件的环面空间拓扑 T^3 对应的爱因斯坦-希尔伯特作用量 (2) 可约化为超空间作用量:

$$S[v] = \int \mathrm{d}t \left[\frac{1}{G} \frac{\dot{v}^2}{v} + \lambda v \right], \tag{30}$$

where $\dot{v}$ denotes the time derivative of $v(t)$ and G can be viewed as proportional to the gravitational constant. The action (30) is very similar to the minisuperspace action of Hartle and Hawking [6]. Clearly, the minimum of the action (30) is achieved for the constant spatial volume profile $v(t) = \frac{V_4}{T}$, where V_4 is the fixed total four-volume and T is the time extent.

其中 $\dot{v}$ 表示 $v(t)$ 对时间的导数，G 可视为与引力常数成正比。作用量 (30) 与哈特-霍金的超空间作用量非常相似 [6]。显然，作用量 (30) 的最小值出现在空间体积恒定的轮廓 $v(t) = \frac{V_4}{T}$ 处，其中 V_4 是固定的总四维体积，T 是时间延拓范围。

In the discrete picture, the spatial volume $v(t)$ corresponds to the discrete spatial volume n_t defined as the number of tetrahedra in the slice t , where t is the original CDT time coordinate. In CDT, no degrees of freedom are frozen, but rather restricting considerations only to n_t corresponds to integrating out all degrees of freedom except the spatial volume. Nevertheless, the functional form of the effective action in terms of $v(t)$

is the same as that of the Hartle-Hawking minisuperspace model. Indeed, in [8,9,28] it was shown that there exists an effective action of the form (30) describing the average of $v(t)$ and its fluctuations, with an additional potential term $v^{1/3}(t)$ for the spherical spatial topology S^3 and a quantum correction $v^{-3/2}(t)$ for the toroidal spatial topology T^3. The latter correction is weak and can be neglected.

在离散图景中，空间体积 $v(t)$ 对应离散空间体积 n_t，后者定义为切片 t 中的四面体数量，而 t 是原本的 CDT 时间坐标。在 CDT 中，并没有自由度被冻结，仅考虑 n_t 相当于积掉除空间体积外的所有自由度。尽管如此，以 $v(t)$ 表示的有效作用量函数形式与哈特-霍金超空间模型的形式完全一致。事实上，文献 [8,9,28] 已表明，存在形如 (30) 的有效作用量描述 $v(t)$ 的平均值及其涨落，其中对球空间拓扑 S^3 附加了势项 $v^{1/3}(t)$，对环面空间拓扑 T^3 附加了量子修正 $v^{-3/2}(t)$。后者修正很弱，可以忽略。

In the spirit of the minisuperspace action, let us now couple a spatially homogeneous and isotropic scalar field to the geometry. The scalar field ϕ is assumed to be constant on a surface of constant time t and depend only on t. Furthermore, let $\phi(t)$ have winding number one and change by δ when going around the universe in the time direction. The minisuperspace action (30) that includes the matter action (5) under the above assumptions can be written for the toroidal spatial topology as

遵循超空间作用量的思路，我们现在将一个空间均匀各向同性的标量场耦合到几何上。假设标量场 ϕ 在恒定时间 t 的曲面上为常数，且仅依赖于 t。此外，设 $\phi(t)$ 的缠绕数为 1，当沿时间方向环绕宇宙一周时，其变化量为 δ。包含上述假设下物质作用量 (5) 的超空间作用量 (30) 对环面空间拓扑可写为

$$S[v,\phi]=\int_{-T/2}^{T/2}\mathrm{d}t\left[\frac{1}{G}\frac{\dot{v}^2}{v}+v\dot{\phi}^2+\lambda v+\kappa\dot{\phi}\right]. \tag{31}$$

The time integration is from $-T/2$ to $T/2$, since the time extent of the CDT universe is fixed to be T, and finally, periodicity in the time direction is assumed, again in agreement with the setup of the computer simulations. The part involving only $v(t)$ is just the Hartle-Hawking minisuperspace action (30), while the part involving $\phi(t)$ consists of two terms. The first term is the kinetic term for a scalar field $\phi(t)$ coupled to the minisuperspace metric $\mathrm{d}s^2=\mathrm{d}t^2+a^2(t)\sum_i \mathrm{d}x_i^2$ with flat coordinates on the spatial three-torus. The second term contains the Lagrange multiplier κ and is added to ensure that the constraint $\phi(T/2)=\phi(-T/2)+\delta$ is met. Similarly, λ in (30) and (31) is not really the cosmological constant, but a Lagrange multiplier, which ensures that the four-volume of the universe is fixed at V_4. This is in order to agree with the computer simulations where the total four-volume is kept constant. In summary, the two Lagrange multipliers λ and κ are introduced to enforce constraints:

时间积分区间为从 $-T/2$ 到 $T/2$，这是因为 CDT 宇宙的时间范围被固定为 T，且最终我们假定时间方向具有周期性，这同样符合计算机模拟的设定。仅包含 $v(t)$ 的部分就是哈特尔-霍金超空间行动 (30)，而包含 $\phi(t)$ 的部分由两项组成。第一项是标量场 $\phi(t)$ 的动能项，$\phi(t)$ 耦合到带有空间三维环面平坦坐标的超空间度规 $\mathrm{d}s^2=\mathrm{d}t^2+a^2(t)\sum_i \mathrm{d}x_i^2$。第二项包含拉格朗日乘子 κ，其作用是确保约束条件 $\phi(T/2)=\phi(-T/2)+\delta$ 得到满足。同理，(30) 和 (31) 中的 λ 并非真正的宇宙学常数，而是拉格朗日乘子，用于确保宇宙的四体积被固定在 V_4，这是为了匹配总四体积保持恒定的计算机模拟设置。综上，我们引入两个拉格朗日乘子 λ 和 κ 来施加约束:

$$\int_{-T/2}^{T/2} \mathrm{d}t v = V_4 \text{ and } \int_{-T/2}^{T/2} \mathrm{d}t \dot{\phi} = \phi\left(\frac{T}{2}\right) - \phi\left(-\frac{T}{2}\right) = \delta, \tag{32}$$

respectively. The Euler-Lagrange equations for (31) are

分别对应上述两个约束。(31) 式的欧拉-拉格朗日方程为

$$\frac{\mathrm{d}}{\mathrm{d}t}\left(v\dot{\phi}\right) = 0 \text{ and } \frac{1}{G}\left(2\frac{\ddot{v}}{v} - \frac{\dot{v}^2}{v^2}\right) - \dot{\phi}^2 - \lambda = 0, \tag{33}$$

which lead to the following constants of motion

由此可得到以下运动常数

$$v\dot{\phi} = K \text{ and } \frac{1}{G}\dot{v}^2 + K^2 - \lambda v^2 = Ev. \tag{34}$$

Equation (34) has two types of solutions, which extremize the action (31) under constraints (32). The first solution is a constant solution:

(34) 式存在两类解，它们在约束 (32) 下使行动 (31) 取极值。第一类是常数解:

$$v(t) = \frac{V_4}{T} = \text{ const. }, \ \phi(t) = \frac{\delta}{T} \cdot t, \tag{35}$$

for which the action (31) is

对应该解的行动 (31) 为

$$S[v, \phi]|_{\text{const}} = \frac{V_4}{T^2} \cdot \delta^2. \tag{36}$$

The second solution is a blob solution given by a piecewise function with a cosine function:

第二类解是团块解，由含余弦函数的分段函数给出:

$$v(t) = \begin{cases} \varepsilon & \frac{\tau}{2} < |t| \leq \frac{T}{2}, \\ c \cdot \cos\left(\frac{2\pi}{\tau}t\right) + c + \varepsilon & |t| \leq \frac{\tau}{2}. \end{cases} \tag{37}$$

It minimizes the action (31), where, in addition to the constraints (32), we additionally impose the kinematic constraint $v(t) \geq \varepsilon$. By construction, a slice cannot vanish during computer simulations, that is, $v(t) > 0$. There is a cutoff $0 < v_{\min} \ll \frac{V_4}{T}$, which is the minimal number of tetrahedra needed to build a triangulation of a spatial slice T^3. In order to make a comparison with numerical results, we should solve the minisuperspace model with the kinematic constraint $v(t) \geq \varepsilon$. The cosine solution (37) describes a bell-shaped or blob volume profile $v(t)$ with time extent τ, as shown in Fig. 13. In principle, any value of ε in the range $\left[v_{\min}, \frac{V_4}{T}\right]$ could be used in the ansatz (37); however, the corresponding action (31) decreases with decreasing ε, and the smallest possible $\varepsilon = v_{\min}$ was chosen from the beginning. The kinematic constraint is important because if $v(t)$ was allowed to shrink to zero, the field would jump by δ in this region and remain constant outside of it. The piecewise solution (37) consists of a blob with time extent τ and a stalk with time

extent $T-\tau$ and spatial volume ε. The solution $v(t)$ satisfies the equations of motion (33) except at the points $t=\pm\tau/2$ where $\ddot{v}(t)$ jumps. However, $\dot{v}(t)$ is continuous in the whole domain, and one still has the constants of motion (34), with different E's in the two regions, but the same K which should then be used to calculate $\phi(t)$ and, thus, the increase in field in the blob region δ_{blob} and in the constant-volume region δ_{const},

它使作用量 (31) 最小化，除约束条件 (32) 外，我们额外添加了运动学约束 $v(t)\geq\varepsilon$。根据构造，在计算机模拟中切片不会消失，即 $v(t)>0$。存在一个截断 $0<v_{\min}\ll\frac{V_4}{T}$，它是构造空间切片三角剖分所需的最少四面体数量 T^3。为了与数值结果对比，我们需要求解带运动学约束 $v(t)\geq\varepsilon$ 的超空间模型。余弦解 (37) 描述了钟形或团块体积轮廓 $v(t)$，其时间延展为 τ，如图 13 所示。原则上，ansatz(37) 中 ε 可取范围 $\left[v_{\min},\frac{V_4}{T}\right]$ 内的任意值；但相应的作用量 (31) 会随 ε 减小而降低，因此我们从一开始就选择了最小的可能值 $\varepsilon=v_{\min}$。运动学约束十分重要，因为如果允许 $v(t)$ 收缩至零，场会在该区域发生 δ 的跳变，在区域外保持恒定。分段解 (37) 由一个时间延展为 τ 的团块和一个时间延展为 $T-\tau$、空间体积为 ε 的柄组成。解 $v(t)$ 除 $\ddot{v}(t)$ 发生跳变的点 $t=\pm\tau/2$ 外，满足运动方程 (33)。不过 $\dot{v}(t)$ 在整个定义域内连续，运动常数 (34) 仍然成立，两个区域的 E 不同，但 K 相同，可用于计算 $\phi(t)$，进而得到团块区域 δ_{blob} 和恒定体积区域 δ_{const} 的场增量，

$$\begin{aligned}\delta_{\text{blob}}&=\frac{K\tau}{\sqrt{\varepsilon(2c+\varepsilon)}}=\frac{2\pi}{\sqrt{G}},\\ \delta_{\text{const}}&=\frac{K(T-\tau)}{\varepsilon},\end{aligned}\tag{38}$$

where $\delta=\delta_{\text{blob}}+\delta_{\text{const}}$.

其中 $\delta=\delta_{\text{blob}}+\delta_{\text{const}}$。

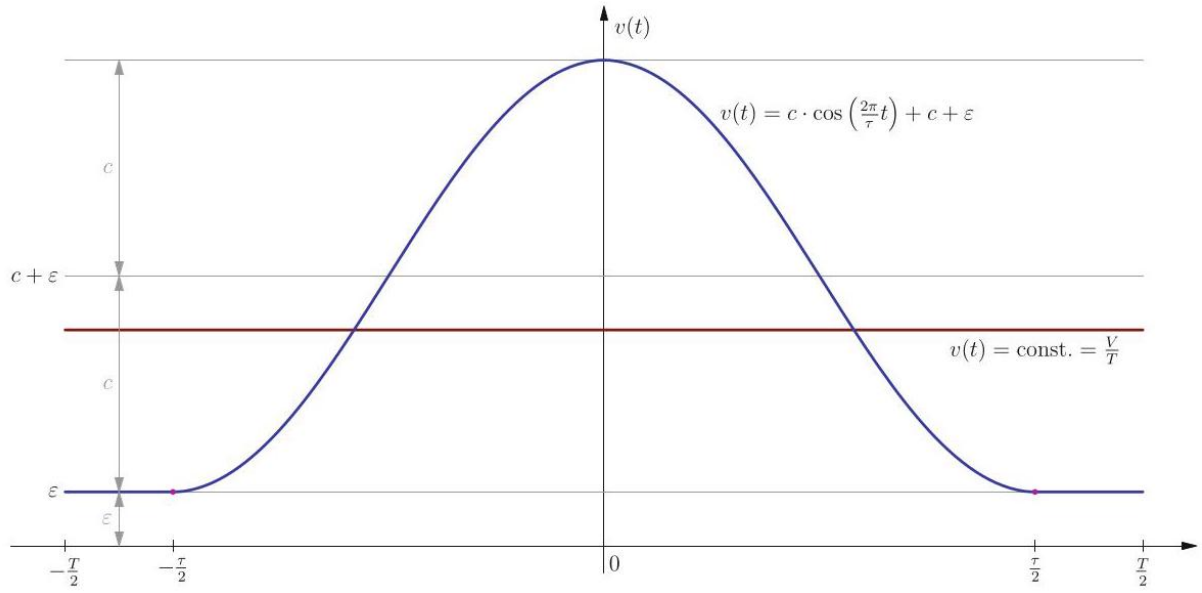

Fig. 13 The constant (red) and cosine (blue) solutions which minimize the minisuperspace action including the scalar field contribution (31)

图 13 使包含标量场贡献的超空间作用量 (31) 最小化的常数解 (红色) 和余弦解 (蓝色)

For $\delta = \delta_{\text{crit}} = \frac{2\pi}{\sqrt{G}}$, the cosine part is stretched over the entire range, i.e., $\tau = T$. The length of the stalk part grows with increasing δ. The expansion of the action (31) calculated for the blob solution (37) in $\delta - \delta_{\text{crit}}$ is given by

对于 $\delta = \delta_{\text{crit}} = \frac{2\pi}{\sqrt{G}}$，余弦部分延伸覆盖了整个范围，即 $\tau = T$。柄部分的长度随 δ 增大而增加。针对团块解 (37) 计算得到的作用量 (31) 在 $\delta - \delta_{\text{crit}}$ 下的展开式为

$$S[v,\phi]|_{\text{blob}} = S_{\text{crit}} \cdot \left[1 + \sqrt{\frac{8T\varepsilon}{V_4}} \cdot \frac{\delta - \delta_{\text{crit}}}{\delta_{\text{crit}}}\right] + o\left((\delta - \delta_{\text{crit}})^2\right), \tag{39}$$

where $S_{\text{crit}} = \frac{4\pi^2}{G}\frac{V_4}{T^2}$.

其中 $S_{\text{crit}} = \frac{4\pi^2}{G}\frac{V_4}{T^2}$。

As shown in Fig. 14, the constant solution (35) has the lowest action when $\delta < \delta_{\text{crit}}$, while the blob solution (37) has the lowest action for $\delta > \delta_{\text{crit}}$. This is in agreement with the earlier observation that for a small jump magnitude δ, below the critical value δ_{crit}, the geometric part of the action prevails, and generic triangulations in the path integral are quite similar to those that dominate when no matter field is present. That is, the matter part of the action is subleading, and the scalar field does not affect the flat volume profile characteristic for the semiclassical phase *C* of four-dimensional Causal Dynamical Triangulations with toroidal spatial topology and without scalar fields.

如图 14 所示，当 $\delta < \delta_{\text{crit}}$ 时，常数解 (35) 的作用量最小，而当 $\delta > \delta_{\text{crit}}$ 时，团块解 (37) 的作用量最小。这与我们之前的观测一致: 当跳变幅度 δ 较小，低于临界值 δ_{crit} 时，作用量的几何部分占主导，路径积分中的一般三角剖分与无物质场时的主导三角剖分十分相似。也就是说，作用量的物质部分是次导的，标量场不会改变四维因果动态三角剖分 (环面空间拓扑、无标量场) 半经典相位 *C* 特有的平坦体积轮廓。

Again, according to the aforementioned remark, we expect that for a sufficiently large value of δ, the matter part of the action will overpower the geometric part, and a bell-shaped volume profile will emerge. Indeed, for $\delta > \delta_{\text{crit}}$, the total action (31), including both geometric and matter terms, is minimal for the generalized pinched solution (37) which is a piecewise combination of a constant function and a cosine function. The scalar field induces a new type of phase transition, where the effective spacetime topology changes from toroidal to a simply connected one. This simple minisuperspace model predicts a first-order phase transition at $\delta = \delta_{\text{crit}}$.

同样，根据上述结论，我们预期当 δ 足够大时，作用量的物质部分将强过几何部分，最终会形成钟形体积轮廓。实际上，对于 $\delta > \delta_{\text{crit}}$，同时包含几何项和物质项的总作用量 (31) 在广义收缩解 (37) 处取得最小值，该解是常数函数与余弦函数的分段组合。标量场会诱发一类新的相变，使有效时空拓扑从环面变为单连通拓扑。这个简单的超空间模型预测一阶相变发生在 $\delta = \delta_{\text{crit}}$。

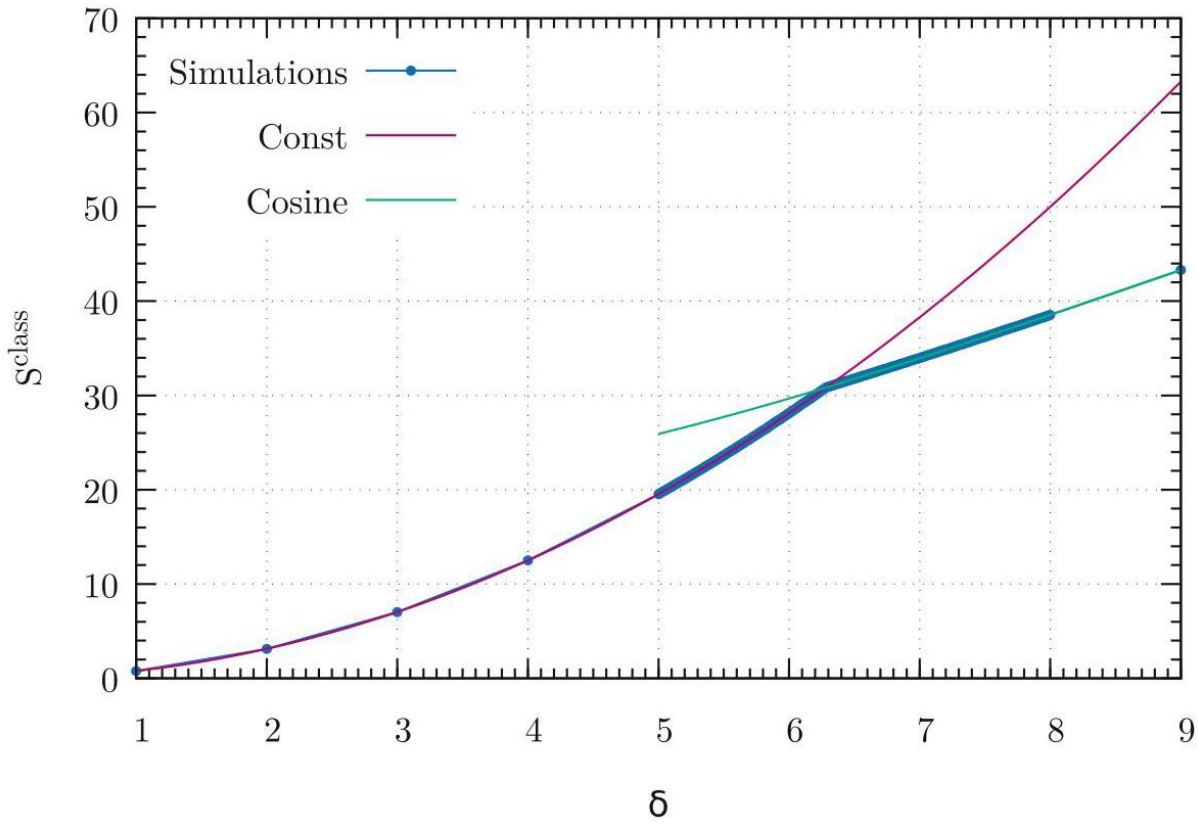

Fig. 14 Plot of the action (31) for constant (red) and cosine (green) solutions. Blue dots denote the value of the action for the classical solution which minimizes the action

图 14 常数解 (红色) 与余弦解 (绿色) 的作用量 (31) 绘图。蓝色点表示使作用量最小的经典解对应的作用量数值

A dynamical scalar field with winding number one in time direction in circle S^1 of circumference δ favors pinched geometries with regions of minimal spatial volume, where the field can change quickly, yet with a minor contribution to the action. There is a competition between the matter part and the geometric part of the action. Pinched triangulations have the smallest matter action, but, in general, the geometric Regge (Einstein-Hilbert) action is larger for them than for non-pinched triangulations.

周长为 δ 的圆 S^1 上，时间方向缠绕数为 1 的动力学标量场更支持收缩几何，这类几何存在极小空间体积区域，标量场可在该区域快速变化，同时对作用量的贡献很小。作用量的物质部分与几何部分存在竞争关系。收缩三角剖分的物质作用量最小，但一般而言，这类三角剖分的几何里奇 (爱因斯坦-希尔伯特) 作用量比非收缩三角剖分更大。

It is most noteworthy that average volume profiles $\langle n_t \rangle$, obtained after integrating out all degrees of freedom but the scale factor, are so well explained by the simple minisuperspace approximation, where the time-dependent scale factor is the only dynamical variable, despite the fact that the CDT model is fully non-perturbative and includes all microscopic degrees of freedom. This agreement is visible when comparing Fig. 12, which presents average volume profiles for various jump magnitudes δ measured in Monte Carlo simulations of the CDT model, and Fig. 13, which depicts classical solutions of the minisuperspace model.

特别值得注意的是，积去所有自由度、仅保留标度因子后得到的平均体积轮廓 $\langle n_t \rangle$，可以被简单的微超空间近似很好地解释——在该近似中，含时标度因子是唯一的动力学变量，即便 CDT 模型本身是完全非微扰的、包含所有微观自由度。这种一致性在对比图 12 和图 13 时清晰可见: 图 12 给出了 CDT 模型蒙特卡洛模拟中测得的、不同跃变幅度 δ 对应的平均体积轮廓，图 13 则描绘了微超空间模型的经典解。

Scalar Fields with Jumps in Spatial Directions

空间方向带跃变的标量场

This section presents results of the CDT model with three dynamical scalar fields with jumps in spatial directions [21, 26]. Configurations generated in the Monte Carlo simulations are now equipped with three nonequivalent and non-contractible three-dimensional hypersurfaces. Each hypersurface is orthogonal to one of the three independent non-contractible loops winding around the toroidal spatial directions x, y , or z . For each hypersurface, there is a corresponding dynamical scalar field ϕ^x, ϕ^y , or ϕ^z with a jump of magnitude δ_x, δ_y , or δ_z when crossing the hypersurface. In general, the jump sizes $\delta_x, \delta_y, \delta_z$ could be chosen independently; however, we will consider only the case $\delta_x = \delta_y = \delta_z = \delta$. Therefore, one can view the systems as having three scalar fields, each taking values in a circle of circumference δ and having winding number one. The results presented were obtained for systems at the same point ($\kappa_0 = 4.0, \Delta = 0.2$) in the semiclassical phase C with the total volume $N_{41} = 720$k and the number of time slices $T = 20$.

本节展示了含三个空间方向跃变动力学标量场的 CDT 模型结果 [21, 26]。蒙特卡洛模拟生成的构型包含三个不等价且不可收缩的三维超曲面。每个超曲面对应环绕环面空间方向 x, y 或 z 的三个独立不可收缩回路之一，且与回路正交。穿过每个超曲面时，对应的动力学标量场 ϕ^x, ϕ^y 或 ϕ^z 会发生幅度为 δ_x, δ_y 或 δ_z 的跃变。一般而言，跃变幅度 $\delta_x, \delta_y, \delta_z$ 可独立选取，但本文仅讨论 $\delta_x = \delta_y = \delta_z = \delta$ 的情况。因此可将该系统视为包含三个标量场，每个标量场的取值位于周长为 δ 的圆上，卷绕数为 1。本文展示的结果均取自半经典相 C 中同一点 ($\kappa_0 = 4.0, \Delta = 0.2$) 处的系统，总容积为 $N_{41} = 720$k ，时间切片数量为 $T = 20$ 。

We can gain information about the influence of dynamical scalar fields with a certain jump magnitude on the geometric structure by repeating the analysis of section ”Classical Scalar Fields.” The system has three scalar fields with three jumps in all three spatial directions. The boundaries x, y , and z associated with dynamical scalar fields are reused to introduce new independent classical fields $\overline{\phi}^x$, $\overline{\phi}^y$, and $\overline{\phi}^z$, which satisfy Laplace equation (27) with jump magnitude $\delta = 1$ (independent of the jump magnitude of dynamical scalar fields) on those boundaries. Although no hypersurface orthogonal to the time direction or dynamic scalar field with a jump in that direction was added, the classical scalar field $\overline{\phi}^t$ was determined using the slice $t = 1$ of the original CDT proper-time foliation as the jump boundary, as was done in section ”Single Scalar Field with a Jump in the Time Direction.”

我们可以通过重复“经典标量场”小节的分析，得到特定跃变幅度的动力学标量场对几何结构影响的相关信息。该系统包含三个标量场，在全部三个空间方向均存在跃变。与动力学标量场关联的边界 x, y 和 z 被重复利用，引入新的独立经典场 $\overline{\phi}^x, \overline{\phi}^y$ 和 $\overline{\phi}^z$ ，这些场满足拉普拉斯方程 (27)，且在上述边界处存在跃变幅度 $\delta = 1$ (与动力学标量场的跃变幅度无关)。虽然本文并未添加正交于时间方向的超曲面，或是在时间方向带跃变的动力学标量场，但依旧仿照“时间方向带跃变的单个标量场”小节的方法，以原始 CDT 固有时叶层的切片 $t = 1$ 作为跃变边界，确定了经典标量场 $\overline{\phi}^t$ 。

Density maps Similarly as in section ”Density Maps in Harmonic Coordinates,” classical scalar field solutions can be used as coordinates to measure density maps and observe how dynamical scalar fields affect the underlying geometry. Figure 15 presents density maps projected on $\overline{\phi}^t - \overline{\phi}^x$ (left) and $\overline{\phi}^x - \overline{\phi}^y$ (right) planes for configurations in the semiclassical phase $C(\kappa_0 = 4.0, \Delta = 0.2)$ with $T = 20$ and three scalar fields with jumps in all spatial directions. Two top graphs show results for $\delta = 1.0$, while two bottom graphs show results for $\delta = 2.0$. Figure 16 presents density maps for configurations at the same point in the coupling constant space, but for $\delta = 4.0$ (top) and $\delta = 7.0$ (bottom).

密度图与“调和坐标下的密度图”小节类似，我们可以将经典标量场解作为坐标测量密度图，观察动力学标量场对基础几何的影响。图 15 展示了半经典相 $C(\kappa_0 = 4.0, \Delta = 0.2)$ 中 $T = 20$ 处构型的密度投影，投影至 $\overline{\phi}^t - \overline{\phi}^x$ (左) 和 $\overline{\phi}^x - \overline{\phi}^y$ (右) 平面，该构型含三个在所有空间方向带跃变的标量场。上方两幅图为 $\delta = 1.0$ 的结果，下方两幅图为 $\delta = 2.0$ 的结果。图 16 展示了耦合常数空间中同一点处构型的密度图，分别对应 $\delta = 4.0$ (上) 和 $\delta = 7.0$ (下)。

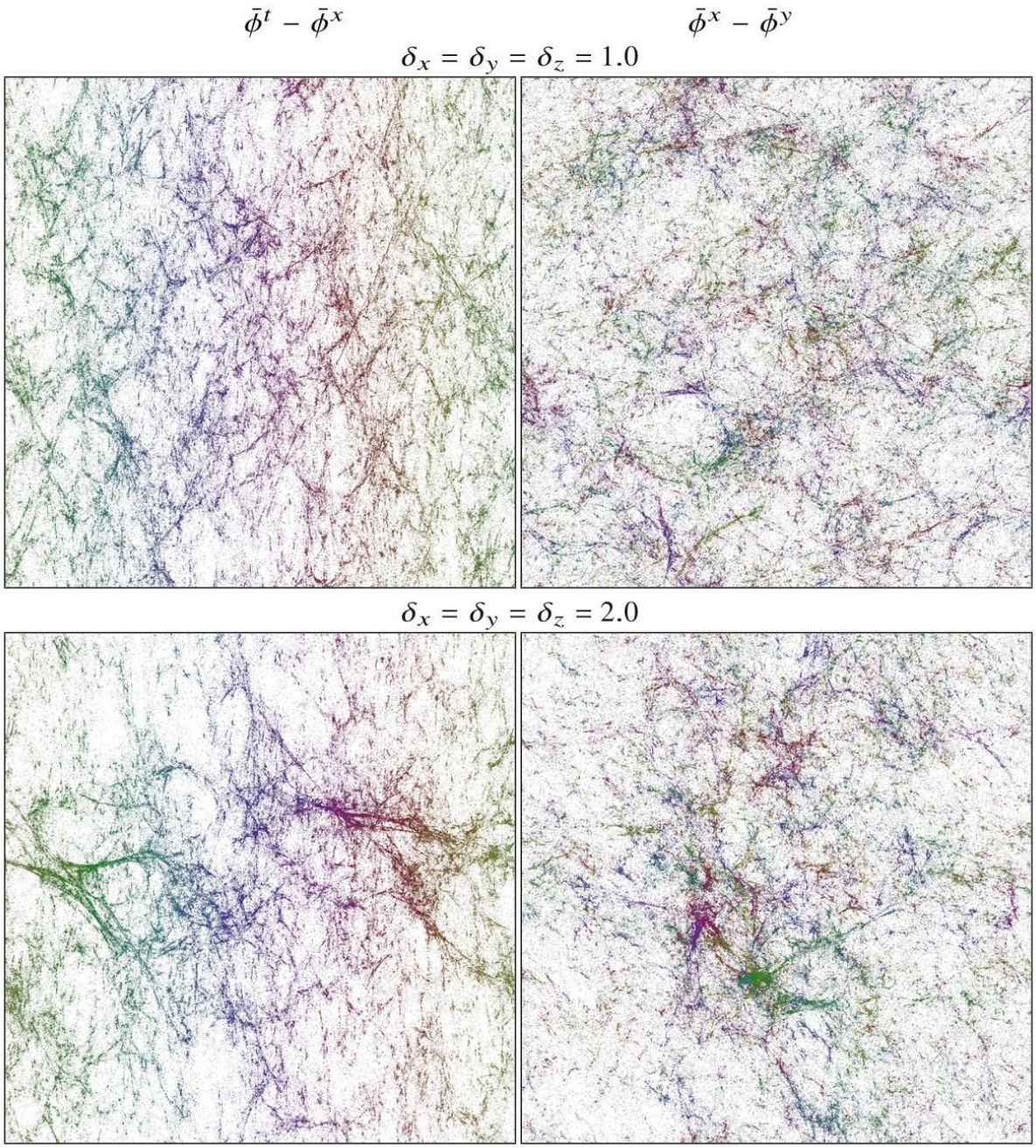

Fig. 15 Density maps projected on $\bar{\phi}^t - \bar{\phi}^x$ (left) and $\bar{\phi}^x - \bar{\phi}^y$ (right) planes for configurations in the semi-classical phase $C\,(\kappa_0 = 4.0, \Delta = 0.2)$ with $T = 20$ and three scalar fields with jumps in all spatial directions with magnitudes $\delta_x = \delta_y = \delta_z = 1.0$ (top) and $\delta_x = \delta_y = \delta_z = 2.0$ (bottom)

图 15 半经典相 $C\,(\kappa_0 = 4.0, \Delta = 0.2)$ 中 $T = 20$ 处构型的密度投影，投影至 $\bar{\phi}^t - \bar{\phi}^x$ (左) 和 $\bar{\phi}^x - \bar{\phi}^y$ (右) 平面，构型含三个在所有空间方向带跃变的标量场，跃变幅度分别为 $\delta_x = \delta_y = \delta_z = 1.0$ (上) 和 $\delta_x = \delta_y = \delta_z = 2.0$ (下)

The following observations can be made from the charts. For small jump magnitudes ($\delta \lesssim 2.0$; see Fig. 15), the cosmic voids and filaments structures are present in all directions. The structures look qualitatively the same as in the pure gravity case (cf. Fig. 8). For medium jump magnitudes ($\delta \approx 4.0$; see the top of Fig. 16),

the density maps qualitatively change as the geometry gets effectively compressed to a single outgrowth in all spatial directions, but not in the time direction. This effect increases in strength with jump magnitude. These results are easily explicable by the pinching phenomenon discussed in section "The Minisuperspace Model." For large jump magnitudes ($\delta \gtrsim 7.0$; see the bottom of Fig. 16), the density maps undergo a qualitative change again. Now the localization is present also in the time direction leading to an effective change of spacetime topology to a four-sphere. This phenomenon is indirectly caused by the transition of spatial topology to a simply connected one and will be explained in section "Topology Change."

可从图中得出以下观测结论。对于小跳跃幅度 ($\delta \lesssim 2.0$ ； 参见图 15)，宇宙空洞与纤维结构在所有方向都存在，结构定性上与纯引力情况完全一致 (参见图 8)。对于中等跳跃幅度 ($\delta \approx 4.0$ ； 参见图 16 上部)，密度图发生定性变化: 几何结构被有效压缩为所有空间方向的单个突出区域，时间方向则不受影响。该效应的强度随跳跃幅度增大而提升，这些结果可以用“微超空间模型”一节讨论的收缩现象轻松解释。对于大跳跃幅度 ($\delta \gtrsim 7.0$ ； 参见图 16 下部)，密度图再次发生定性变化。现在时间方向也出现局域化，导致时空拓扑有效变为四维球面。该现象由空间拓扑向单连通拓扑的转变间接引发，将在“拓扑变化”一节中解释。

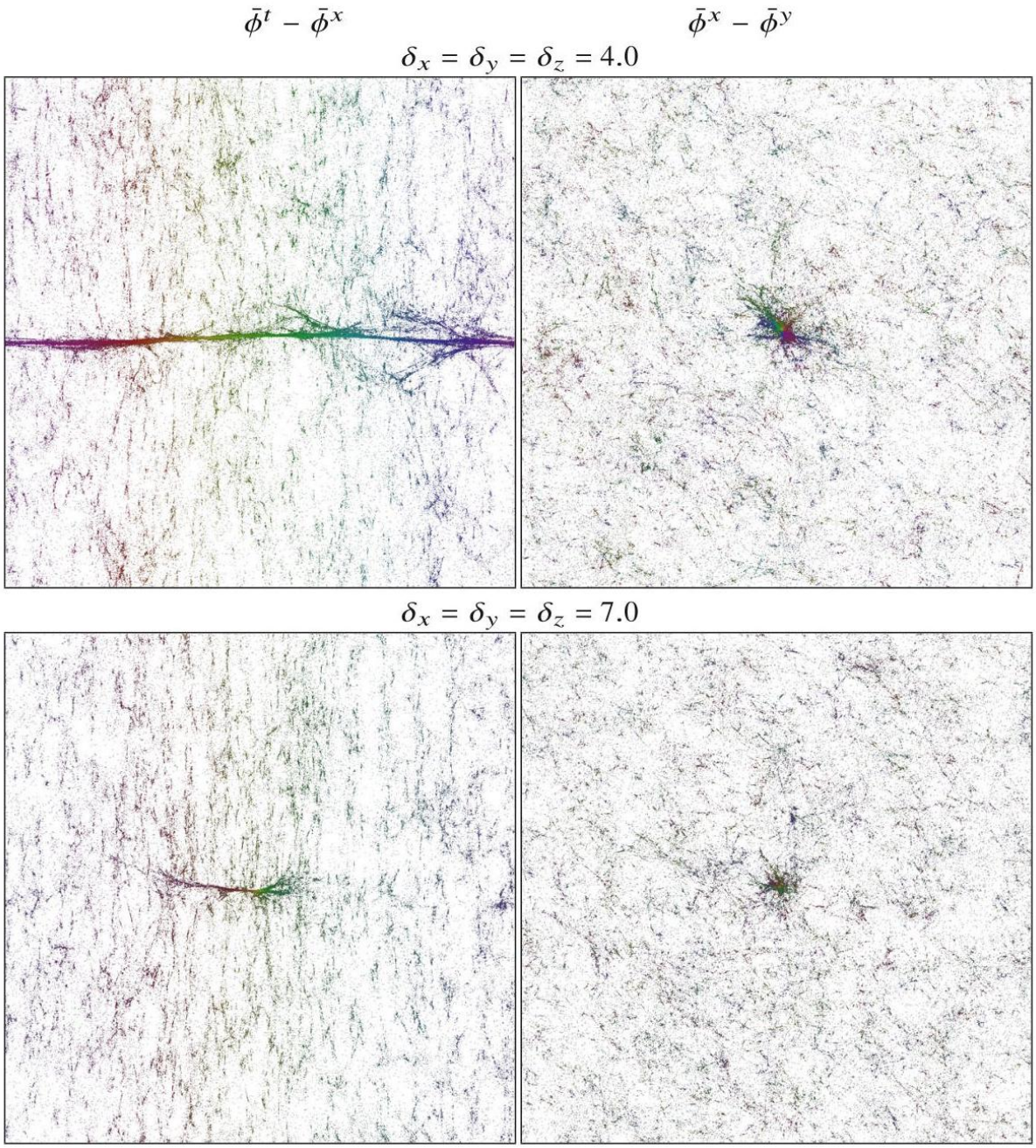

Fig. 16 Density maps projected on $\overline{\phi}^t - \overline{\phi}^x$ (left) and $\overline{\phi}^x - \overline{\phi}^y$ (right) planes for configurations in the semi-classical phase C ($\kappa_0 = 4.0, \Delta = 0.2$) with $T = 20$ and three scalar fields with jumps in all spatial directions with magnitudes $\delta_x = \delta_y = \delta_z = 4.0$ (top) and $\delta_x = \delta_y = \delta_z = 7.0$ (bottom)

图 16 半经典相 C ($\kappa_0 = 4.0, \Delta = 0.2$) 中、满足 $T = 20$ 的构型，以及三个在所有空间方向带有跳跃、幅度分别为 $\delta_x = \delta_y = \delta_z = 4.0$ (上部) 和 $\delta_x = \delta_y = \delta_z = 7.0$ (下部) 的标量场，投影到 $\overline{\phi}^t - \overline{\phi}^x$ (左) 和 $\overline{\phi}^x - \overline{\phi}^y$ (右) 平面的密度图

One could naïvely think that as an effect of the geometry pinching caused by the dynamical scalar fields with large jumps, one would obtain a compactified geometry similar to the geometry of the bifurcation phase C_b or (for even larger jump magnitudes) to a collapsed geometry of the B phase. Interestingly, this is not the

case. For large jump size, magnification of dense regions, associated with spherical outgrowth and visible in Fig. 16 (right), would reveal the fine structure with cosmic voids and filaments characteristic for the semiclassical phase C without scalar fields. Thus, the internal geometry of the large outgrowth created by the pinching effect of the dynamical scalar fields with jumps is completely different from the one observed in phases C_b and B (cf. Figs. 9 and 10 for the case of pure gravity).

人们通常会天真地认为，带大跳跃的动力学标量场引发的几何收缩，会产生类似分岔相 C_b 的紧致几何，若跳跃幅度更大，则会得到 B 相的坍缩几何。有趣的是，实际情况并非如此。对于大跳跃幅度，放大图 16(右) 中可见的、与球形突出区域相关的致密区域，就能发现保留半经典相 C (无标量场) 特征的宇宙空洞与纤维 fine 结构。因此，带跳跃的动力学标量场通过收缩效应形成的大突出区域，其内部几何与在 C_b 相和 B 相中观测到的完全不同 (纯引力情况参见图 9 和图 10)。

Volume profiles in harmonic coordinates The coordinate given by the classical scalar field $\overline{\phi}^{\mu}, \mu = x, y, z$ can be used to define a three-dimensional hypersurface $H\left(\overline{\phi}^{\mu}\right)$ at position $\overline{\phi}^{\mu}$ and orthogonal to direction μ. The boundary consists of tetrahedral faces shared by two four-simplices, where the value of the classical field is lower than $\overline{\phi}^{\mu}$ for one simplex and greater than or equal to $\overline{\phi}^{\mu}$ for the other simplex (taking into account periodicity), that is, the two simplices lie on two opposite sides of the boundary. Such boundaries form three-dimensional hypersurfaces with topology T^3 . For example, a boundary orthogonal to the direction x would be represented by a vertical line (cross section) corresponding to a constant value of $\overline{\phi}^{x}$ on the right graphs of Fig. 15. For a given hypersurface corresponding to $\overline{\phi}^{\mu}$, one can measure its volume $N\left(\overline{\phi}^{\mu}\right)$, defined as the number of tetrahedra belonging to the boundary, making it possible to measure the boundary volume profiles not only in time but also in spatial directions. Volume profiles $N\left(\overline{\phi}^{\mu}\right)$ provide information on the geometric properties of a triangulation.

调和坐标下的体积轮廓经典标量场 $\overline{\phi}^{\mu}, \mu = x, y, z$ 给出的坐标可用于定义位置 $\overline{\phi}^{\mu}$ 处、正交于 μ 方向的三维超曲面 $H\left(\overline{\phi}^{\mu}\right)$。边界由两个四维单形共享的四面体面构成: 考虑周期性后，一个单形的经典场值小于 $\overline{\phi}^{\mu}$ ，另一个大于等于 $\overline{\phi}^{\mu}$ ，即两个单形分别位于边界的对侧。这类边界构成拓扑为 T^3 的三维超曲面。例如，正交于 x 方向的边界，对应图 15 右侧图中 $\overline{\phi}^{x}$ 取常数的竖直线 (横截面)。对于对应 $\overline{\phi}^{\mu}$ 的给定超曲面，可以测量其体积 $N\left(\overline{\phi}^{\mu}\right)$，体积定义为属于边界的四面体数量，因此我们不仅可以测量时间方向的边界体积轮廓，也可以测量空间方向的。体积轮廓 $N\left(\overline{\phi}^{\mu}\right)$ 可以提供三角剖分几何性质的相关信息。

Figure 17 presents boundary volume profiles $N\left(\overline{\phi}^{\mu}\right), \mu = x, y, z$ for configurations in the semiclassical phase C with scalar fields with jumps $\delta = 1, 2, 4$, and 7 in all three spatial directions. As predicted by the minisuperspace model described in section "The Minisuperspace Model," volume profiles $N\left(\overline{\phi}^{\mu}\right)$ are visibly pinched and localized for large jump magnitudes.

图 17 给出了半经典相 C 中，存在带跃变标量场 $\delta = 1, 2, 4$ 且三个空间方向跃变幅度均为 7 的组态的边界体积轮廓 $N\left(\overline{\phi}^{\mu}\right), \mu = x, y, z$。正如“超空间模型”章节所述的微超空间模型所预测，对于大跃变幅度，体积轮廓 $N\left(\overline{\phi}^{\mu}\right)$ 会出现明显收缩并局域化。

Spatial volume profiles Spatial volume profiles n_t for configurations in the semiclassical phase C ($\varkappa_0 = 4.0, \Delta = 0.2$) for $T = 20$ with dynamical scalar fields with jumps $\delta = 1.0, 2.0, 4.0$, and 7.0 in all three spatial directions are shown in Fig. 18. Blue bars denote a volume profile n_t for a single generic configuration, while red lines

denote the volume profile $\langle n_t \rangle$ averaged over many Monte Carlo configurations. For $\delta \gtrsim 4.0$, a pinching takes place, and the phase transition leads to an effective change in the spacetime topology from the toroidal to the spherical one. In the bottom-right chart of Fig. 18 for $\delta = 7.0$, one can observe a volume profile with a stalk and a blob part. Remarkably, the average spatial volume profile $\langle n_t \rangle$ is well fitted by the cosine-cubed function of the proper-time t characteristic for the pure gravity de Sitter solution observed in phase C_{dS} , where spherical spatial topology was put in by hand. Moreover, for δ above the critical value, the average spatial volume profiles $\langle n_t \rangle$ seem to be quite universal, changing only a little with δ .

空间体积轮廓图 18 展示了半经典相 $C\,(\kappa_0 = 4.0, \Delta = 0.2)$ 中，$T = 20$ 存在带跃变动力学标量场 $\delta = 1.0, 2.0, 4.0$ 且三个空间方向跃变幅度均为 7.0 的组态的空间体积轮廓 n_t 。蓝色柱代表单个一般组态的体积轮廓 n_t ，红色线代表对大量蒙特卡洛组态平均得到的体积轮廓 $\langle n_t \rangle$ 。对于 $\delta \gtrsim 4.0$ ，会发生收缩，相变导致时空拓扑从环形有效转变为球形。在图 18 右下角对应 $\delta = 7.0$ 的图中，可以观察到体积轮廓分为柄状和团状两部分。值得注意的是，平均空间体积轮廓 $\langle n_t \rangle$ 可以很好地由固有时 t 的余弦三次方函数拟合，该函数是相 C_{dS} 中观测到的纯引力德西特解的特征，该相人为预设了球形空间拓扑。此外，当 δ 高于临界值时，平均空间体积轮廓 $\langle n_t \rangle$ 表现出很强的普适性，随 δ 的变化很小。

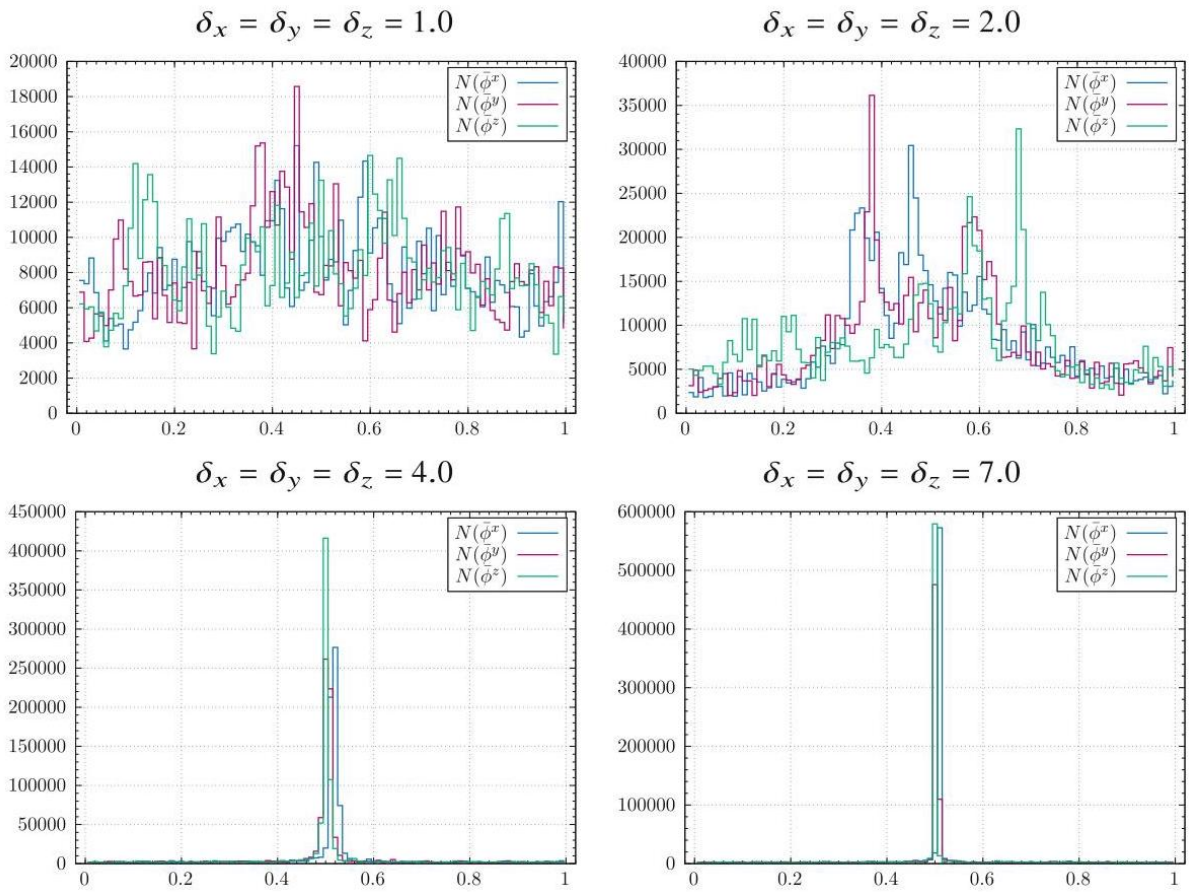

Fig. 17 Boundary volume profiles $N\left(\overline{\phi}^{x}\right), N\left(\overline{\phi}^{y}\right)$ and $N\left(\overline{\phi}^{z}\right)$ in coordinates defined by classical scalar fields for the same configurations as in Figs. 15 and 16 with dynamical scalar fields with a jump $\delta = 1.0, 2.0, 4.0$, and 7.0 in all spatial directions

图 17 与图 15 和图 16 构型相同，具有带跳变 $\delta = 1.0, 2.0, 4.0$ 动力学标量场的经典标量场定义坐标下的边界体积轮廓 $N\left(\overline{\phi}^{x}\right), N\left(\overline{\phi}^{y}\right)$ 和 $N\left(\overline{\phi}^{z}\right)$，所有空间方向取值均为 7.0

Topology Change

拓扑改变

Numerical Monte Carlo simulations performed for $N_{41} = 720\text{k}$ and $T = 20$ suggest that coupling quantum geometry to scalar fields with nontrivial boundary conditions can lead to a new type of phase transition. For globally hyperbolic spacetime with a toroidal spatial topology and scalar fields with matching topological boundary conditions and sufficiently strong coupling (jump magnitude δ in our model), a phase transition is observed that leads to an effective change from a toroidal topology to a simply connected one. The mechanism is schematically illustrated in Fig. 19. on a simple two-dimensional example, where a fractal geometry can be compared to a toroidal balloon with outgrowths. For the pure gravity case and for a small jump magnitude, the geometry typically looks like in the left plot with a large central part and a number of relatively small outgrowths. Dynamical scalar fields with large jump magnitudes compress the central part, where (almost) all change of the field occurs, and, because of the total volume constraint, transfer the volume into one large outgrowth, where the field is much more uniform, resulting in the picture on the right plot. The dominating toroidal part with many nontrivially correlated almost spherical outgrowths changes into the dominating spherical part with many outgrowths and a single toroidal outgrowth of cutoff size, which is needed due to the global topological restrictions imposed.

针对 $N_{41} = 720\text{k}$ 和 $T = 20$ 开展的数值蒙特卡罗模拟表明，将量子几何与带有非平凡边界条件的标量场耦合会产生一类新型相变。对于具有环面空间拓扑、且标量场满足匹配拓扑边界条件、耦合足够强 (我们模型中跃迁幅度为 δ) 的整体双曲时空，观测到的相变会让有效拓扑从环面拓扑变为单连通拓扑。其机制在图 19 的一个简单二维示例中得到了示意性展示，该示例中可将分形几何类比为带有赘生结构的环面气球。对于纯引力情况和跃迁幅度较小的情况，几何通常如左图所示: 存在一个大的中心区域，以及若干相对较小的赘生结构。带有大幅跃迁幅度的动力学标量场会压缩 (几乎) 全部场变化发生的中心区域，并且由于总体积约束，会将体积转移到场均匀度高得多的一个大赘生结构中，最终得到右图的图景。带有大量非平凡关联近球形赘生结构的主导环面部分，转变为带有大量赘生结构和一个截断尺寸单环面赘生结构的主导球形部分，这一结果是由施加的整体拓扑约束决定的。

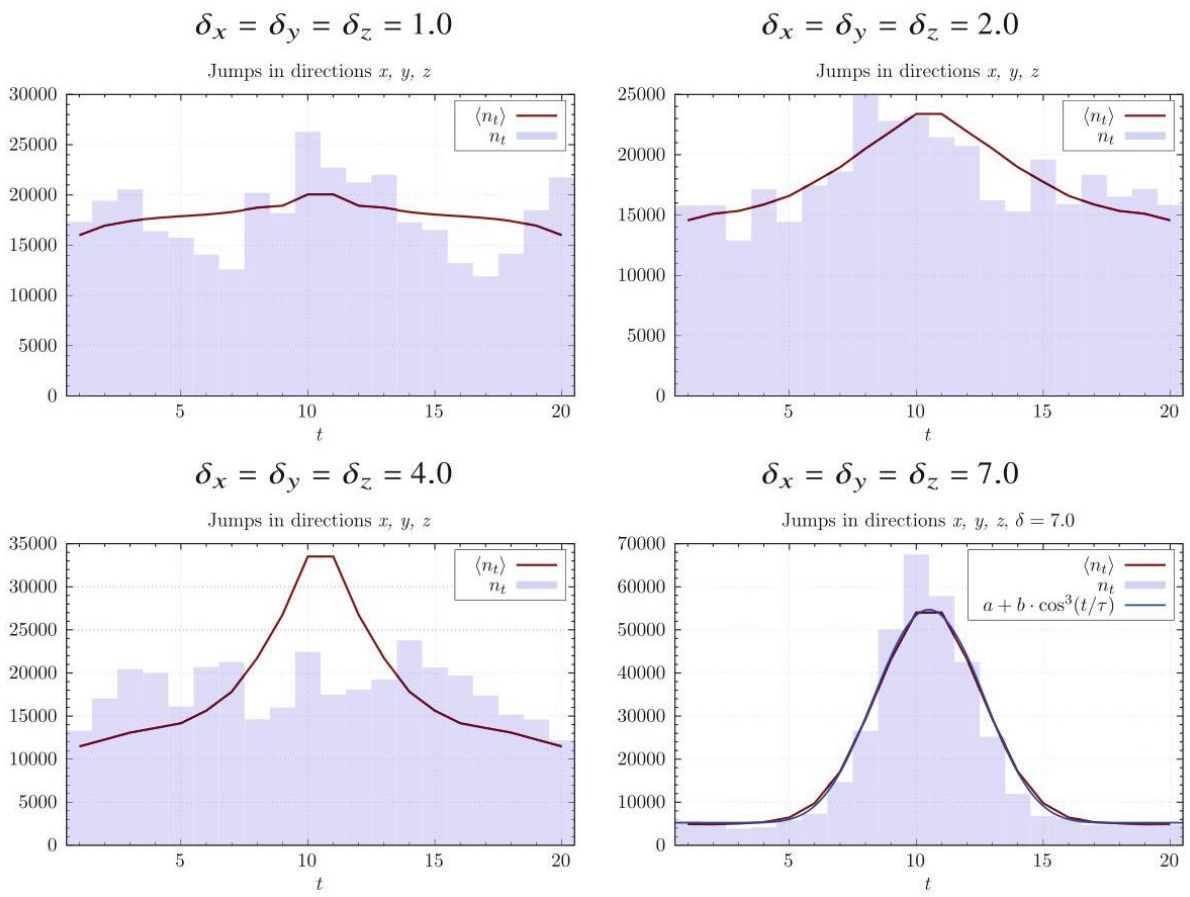

Fig. 18 Spatial volume profiles n_t for a single generic configuration (blue bars) and averaged over configurations (red line) inside the semiclassical phase C ($\kappa_0 = 4.0, \Delta = 0.2$) for $T = 20$ with dynamical scalar fields with jump $\delta = 1.0, 2.0, 4.0$, and 7.0 in all spatial directions

图 18 半经典相 C ($\kappa_0 = 4.0, \Delta = 0.2$) 中，$T = 20$ 分别在单个一般构型 (蓝色柱) 和构型平均 (红色线) 下的空间体积剖面 n_t ， 该系统耦合带有跃迁 $\delta = 1.0, 2.0, 4.0$ 的动力学标量场，所有空间方向取值为 7.0

The process of a transition from toroidal (T^4) to spherical (S^4) topology of the four-dimensional spacetime caused by scalar fields is twofold. First, dynamical scalar fields winding once around a circle in all three spatial directions bring a pinching of the geometry in spatial directions and lead to a spatial topology change into a simply connected one. This effect is explained by the minisuperspace model discussed in section "The Minisuperspace Model." Second, a morphed spatial topology triggers a change in the potential term of the effective action for n_t , causing a pinching of the geometry in the time direction [9,14]. For CDT with spherical spatial topology, the averaged spatial volume profile $\langle n_t \rangle$ is given by a cosine-cubed function in the de Sitter phase C_{dS} . This explains the shape of the plot of $\langle n_t \rangle$, shown in Fig. 18 (bottom right), in the case of toroidal spatial topology with dynamical scalar fields with a large jump in spatial directions.

标量场引发的四维时空从环面 (T^4) 拓扑到球形 (S^4) 拓扑的转变过程分为两部分。首先，绕全部三个空间方向各环绕一周的动力学标量场会造成空间方向的几何收缩，引发空间拓扑转变为单连通拓扑。该效应已在“迷你超空间模型”一节讨论的迷你超空间模型中得到解释。其次，变形后的空间拓扑会触发 n_t 有效作用量的势项发生改变，引发时间方向的几何收缩 [9,14]。对于具有球形空间拓扑的因果动力学三角剖分，德西特相 C_{dS} 中的平均空间体积剖面 $\langle n_t \rangle$ 由三次余弦函数给出。这解释了图 18(右下) 中，带有空间方向大幅跃变动力学标量场的环面空间拓扑情况下，$\langle n_t \rangle$ 的曲线形状。

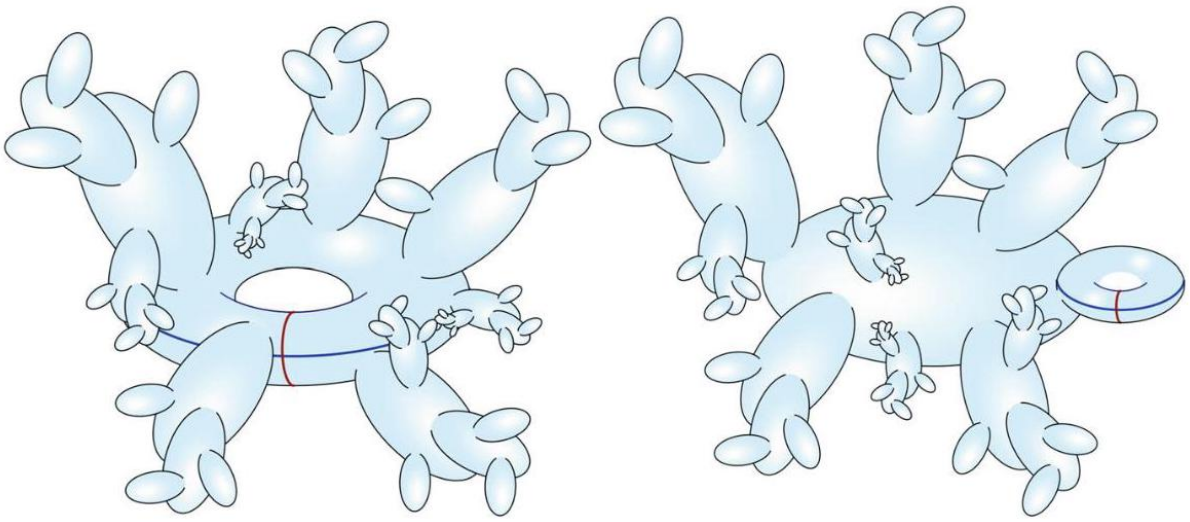

Fig. 19 Two-dimensional illustrations representing the generic features of CDT quantum geometries for the pure gravity case / a small jump magnitude (left) and for a large jump magnitude (right)

图 19 展示了不同情况下 CDT 量子几何一般特征的二维示意图: 纯引力/小跃迁幅度 (左) 和大跃迁幅度 (右)

The three-volume of a stalk is of the cutoff size for the original pure gravity CDT with imposed spherical spatial topology, while it is significantly larger for the toroidal CDT coupled to scalar fields with jumps (causing the effective change in spatial topology). This is probably due to a bigger minimal three-dimensional toroidal triangulation [9]. At any rate, the existence of the stalk is a finite-size effect related to the fixed spacetime topology conditions imposed in the MC simulations, which cannot change regardless of the effective topology change and becomes negligible in the large-volume limit. Therefore, the results presented above strongly support our conjecture that the newly observed phase transition leads to an effective spatial topology change.

对于施加球形空间拓扑约束的原始纯引力 CDT，茎秆的三维体积为截断尺度大小；而对于耦合了带跃变标量场的环面 CDT(引发有效空间拓扑改变)，其茎秆体积显著更大。这很可能源于更大的最小三维环面三角剖分 [9]。无论如何，茎秆的存在是与 MC 模拟中施加的固定时空拓扑条件相关的有限尺寸效应，该条件不会随有效拓扑改变而变化，在大体积极限下可以忽略。因此，上述结果有力支持了我们的猜想: 新观测到的相变会引发有效的空间拓扑改变。

Conclusions

结论

Causal Dynamical Triangulations model is a model of generic geometry fluctuations at the Planck scale and a promising candidate for a theory of quantum gravity. It provides a lattice regularization of the formal gravitational path integral, which makes it feasible to use Monte Carlo simulations to study properties of a typical quantum universe, that one might expect before a possible period of inflation.

因果动态三角割分模型是描述普朗克尺度下一般几何涨落的模型，也是量子引力理论颇具前景的候选方案。它为形式化引力路径积分提供了格点正则化，使得我们可以利用蒙特卡洛模拟研究典型量子宇宙的性质——这正是我们可能在可能的暴胀时期之前预期会存在的性质。

Configurations generated in computer simulations of the CDT model are delivered as geometries that are coordinate-free in spatial directions. While this seems desirable from a GR point of view, there are, indeed, cases when coordinates can be very useful. The reason we were able to construct an effective action for the scale factor [10,14] was precisely that we had a coordinate in the time direction at our disposal. Also, when studying phase transitions, an ensemble of observables might shed some light on geometric fluctuations, and, often, it is worthwhile to have a coordinate system available. In this chapter we have tried to construct such a coordinate system along spatial directions and use it to better understand the geometry of configurations and to address the question of formulating an effective measure that would cover all spacetime directions.

CDT 模型计算机模拟生成的构型是空间方向无坐标的几何。从广义相对论的角度来看，这一点似乎很理想，但确实，在很多情况下坐标是非常有用的。我们之所以能为标度因子构造有效作用量[10,14]，正是因为我们已经有了时间方向的坐标。此外，在研究相变时，一组可观测量或许能为几何涨落提供启示，因此拥有可用的坐标系往往很有价值。本章中，我们尝试在空间方向构造这样一个坐标系，并用它更好地理解构型的几何，解决构造覆盖全时空方向的有效测度这一问题。

In the first part, we described how to define harmonic coordinates on CDT triangulations with toroidal spatial topology and time-periodic boundary conditions. This is achieved by taking advantage of the periodic structure of the piecewise linear manifold to introduce four scalar fields that take values in a circle S^1 . Each field winds once around the circle when moving around a non-contractible loop in a given direction. Technically, the field is considered to take values in $\mathbb{R}$, instead of a circle S^1 , but a jump in the field value is introduced when crossing a hypersurface. Given a triangulation $\mathcal{T}$ appearing in the CDT path integral, we define four non-contractible and oriented hypersurfaces orthogonal to one of the four directions. The hypersurfaces, also called boundaries and labeled by x, y, z , and t , are nonequivalent, meaning that it is not possible to continuously deform one into another. The hypersurface t was chosen as the spatial slice with CDT time $t = 1$. Based on these hypersurfaces, we found four harmonic maps $\overline{\phi}^{\mu}, \mu = x, y, z, t$ from $\mathcal{T}$ onto S^1 . The four classical scalar fields satisfy the Laplace equation with nontrivial boundary conditions and are used as spatial coordinates. Such coordinates are a close analogue of the harmonic coordinates used in the context of GR [29], but here we use them for nonclassical, irregular, and highly nontrivial geometries.

在第一部分，我们介绍了如何在具有环面空间拓扑和时间周期边界条件的 CDT 三角割分上定义调和坐标，具体方法是利用分段线性流形的周期结构引入四个取值于圆 S^1 的标量场。当沿给定方向环绕一条不可收缩回路时，每个场绕圆缠绕一周。技术上，该场被认为取值于 $\mathbb{R}$ 而非圆 S^1，但穿越超曲面时会引入场值跳变。给定 CDT 路径积分中出现的三角割分 $\mathcal{T}$，我们定义了四个分别正交于四个方向的不可收缩定向超曲面。这些超曲面也称为边界，由 x, y, z 和 t 标记，二者不对等价，即无法通过连续形变将一个变为另一个。超曲面 t 被选为对应 CDT 时间 $t = 1$ 的空间切片。基于这些超曲面，我们得到了四个从 $\mathcal{T}$ 到 S^1 的调和映射 $\overline{\phi}^{\mu}, \mu = x, y, z, t$。这四个经典标量场满足带非平凡边界条件的拉普拉斯方程，被用作空间坐标。这类坐标是广义相对论框架下所用调和坐标的近似类比 [29]，但我们此处将其用于非经典、不规则且高度非平凡的几何。

An individual spacetime history contributing to the partition function is not an observable, precisely in the same way as a trajectory of a particle in the quantummechanical path integral is not an observable. While it can be measured in computer simulations, this is not the case in the real world due to the quantum nature of the theory. A quantum theory defines an expectation value of an observable, which is suitably averaged over the configurations contributing to the path integral. Nonetheless, a single typical configuration of the path integral might provide interesting information. In some cases, the value of the observable on such a configuration is quite accurate. We display the geometry of a typical quantum universe using the new harmonic coordinates defined by means of four classical scalar fields. The use of such coordinates is well suited to observe outgrowths of a triangulation in a density plot. It is very nontrivial that these ideas can be applied to understand the structures which appear in very irregular and fluctuating geometries. Indeed, such a choice of coordinates seems to be good, in the sense that they preserve the structure of the triangulation and depict fractal outgrowths as dense clouds of points. In the case of configurations from the semiclassical phase C, which is undoubtedly the most interesting phase from the physical point of view, the projections of volume densities to two-dimensional planes reveal web structures surprisingly similar to the well-known structures of cosmic voids and fibers observed in the real present-day Universe. Comparison of the time coordinate defined by the scalar field with the original CDT time t serves as a check of how well this prescription works.

对配分函数有贡献的单个时空历史并非可观测量，这就和量子力学路径积分中粒子的单个运动轨迹不是可观测量完全一样。虽然它可以在计算机模拟中被测量，但由于理论的量子本性，在现实世界中无法做到这一点。量子理论定义可观测量的期望值，该值是对贡献路径积分的所有构型做适当平均得到的。尽管如此，路径积分中的单个典型构型仍能提供有趣的信息，在某些情况下，可观测量在这类构型上的取值相当准确。我们利用四个经典标量场定义的新调和坐标展示了典型量子宇宙的几何。这类坐标非常适合在密度图中观测三角割分的突出结构。这些思路能够用于理解出现在极不规则的涨落几何中的结构，这一点本身就十分不平凡。实际上，这类坐标选择的效果很好: 它保留了三角割分的结构，将分形突出结构描绘为密集的点云。对于半经典相 C 的构型——从物理角度来看这无疑是最有趣的相——体积密度向二维平面的投影呈现出网状结构，其与当今宇宙观测到的著名宇宙空洞-纤维结构惊人地相似。将标量场定义的时间坐标与原始 CDT 时间 t 对比，可以检验该方案的效果。

In computer-generated spacetimes, the filaments are not matter content, but regions where some of the harmonic fields $\overline{\phi}_i^{\mu}$ vary slowly. In terms of geometry, these regions can probably be associated with outgrowths that share a small boundary with the rest of the triangulation. However, the fact that they have a filament structure instead of being randomly conglomerated indicates structures of a certain duration rather than what is depicted in Fig. 7 and is realized in two-dimensional Liouville quantum gravity [30]. This duration is particularly pronounced in the time direction in the upper left picture of Fig. 8. The persistence of the

filament structure is nontrivial and is still not fully understood.

在计算机生成的时空里，这些细丝并非物质组分，而是调和场 $\overline{\phi}_i^{\mu}$ 变化缓慢的区域。从几何角度看，这些区域大概率对应与三角剖分其余部分共享小边界的外延结构。不过，它们呈细丝结构而非随机聚结的事实表明，这是具有一定持续时长的结构，而非图 7 所描绘、二维刘维尔量子引力中实现的那种结构 [30]。在图 8 的左上图像中，这种持续时长在时间方向上尤为显著。细丝结构的持续性并非平凡结论，目前仍未被完全理解。

We hope that measurements of spacetime correlations will allow us to determine experimentally, i.e., using Monte Carlo simulations, the effective continuum action that governs our lattice model not only in time but also in spatial directions. The four harmonic maps $\overline{\phi}_i^{\mu}, \mu = x, y, z, t$ from $\mathcal{T}$ onto S^1 now served as our new coordinates. Constant values of $\overline{\phi}_i^{\mu}$ defined hypersurfaces $H\left(\overline{\phi}^{\mu}\right)$, for which one can measure the boundary volume profiles $N\left(\overline{\phi}^{\mu}\right)$, i.e., the number of tetrahedra belonging to the hypersurface. Furthermore, the volume-volume correlator $C\left(\Delta\overline{\phi}^{\mu}\right)$ between volumes of hypersurfaces separated by distance $\Delta\overline{\phi}^{\mu}$ can be measured, and subsequently the effective action can be reconstructed (see [2] for more details). The calculation works as well with the $\overline{\phi}^{t}$ coordinate as with the original t coordinate. The results for the correlations $C\left(\Delta\overline{\phi}^{\mu}\right), \mu = x, y, z$ in the spatial directions are encouraging, although not as good as those for the time direction [21]. As discussed above, accuracy is limited to what can be obtained from a single configuration, since we are essentially introducing an independent coordinate system for each configuration, but the feasibility of performing superpositions derived from several configurations is conceivable. This idea, which we still need to explore, perhaps for even larger triangulations, would be particularly useful for improving results in spatial directions. It would be really exciting to be able to measure correlators $C\left(\Delta\overline{\phi}_{\mu}\right), \mu = x, y, z$ with good precision.

我们希望通过测量时空关联，能够借助蒙特卡洛模拟从实验层面确定，不仅在时间方向、也能在空间方向上支配我们格点模型的有效连续作用量。四个从 $\mathcal{T}$ 映射到 S^1 的调和映射 $\overline{\phi}_i^{\mu}, \mu = x, y, z, t$ 可作为我们的新坐标。$\overline{\phi}_i^{\mu}$ 的等值定义了超曲面 $H\left(\overline{\phi}^{\mu}\right)$，我们可以测量该超曲面的边界体积剖面 $N\left(\overline{\phi}^{\mu}\right)$，即属于该超曲面的四面体数量。此外，我们可以测量间隔距离 $\Delta\overline{\phi}^{\mu}$ 的超曲面体积之间的体积-体积关联函数 $C\left(\Delta\overline{\phi}^{\mu}\right)$，进而重构出有效作用量 (详见文献 [2])。该计算在 $\overline{\phi}^{t}$ 坐标和原初 t 坐标下都能成立。空间方向关联 $C\left(\Delta\overline{\phi}^{\mu}\right), \mu = x, y, z$ 的结果令人鼓舞，尽管暂不及时间方向的结果理想 [21]。如前文所述，精度受限于单个构形所能达到的水平，因为我们本质上是为每个构形引入了独立的坐标系，但从多个构形得到叠加态是可行的。这一思路仍有待探索，或许可应用于更大规模的三角剖分，它对改善空间方向的结果尤其有用。若能高精度测量关联函数 $C\left(\Delta\overline{\phi}_{\mu}\right), \mu = x, y, z$，将会十分令人振奋。

The classical scalar fields $\overline{\phi}_i^{\mu}$, which were used as coordinates, do not affect the geometry of the underlying spacetime manifold (triangulation). An important aspect that makes the fields independent of the hypersurface used to define them is that they have been mapped to S^1 and not to $\mathbb{R}$. The next step was to investigate a genuine dynamical matter-gravity system in which the scalar field can influence the geometry. As mentioned in the introduction to section "Dynamical Scalar Fields," no considerable effect was observed on the geometry of an ordinary scalar field coupled to gravity, but taking values in R. Seemingly, such a result may be surprising, since matter should have a significant effect on the geometry in GR, but we must remember that the configurations are Wick-rotated to Euclidean spacetimes, where gravity is in some sense repulsive, and also where, for example, the solutions of black holes are completely regular solutions of Einstein's equations

and the mass M appears in them only as a parameter.

用作坐标的经典标量场 $\overline{\phi}_i^{\mu}$ 不会改变底层时空流形 (三角剖分) 的几何。让这些场不依赖于定义它们所用超曲面的一个关键之处在于，它们被映射到 S^1 而非 $\mathbb{R}$ 。下一步我们研究的是真正的动力学物质-引力系统，其中标量场可以影响几何。正如“动力学标量场”小节引言所述，我们并未观测到普通耦合引力、取值在 R 中的标量场对几何产生显著影响。表面上看，这一结果或许令人惊讶，因为广义相对论中物质本应对几何产生显著影响，但我们必须记住，构形已经做了威克旋转成为欧几里得时空，在欧氏时空里引力在某种意义上是排斥性的，而且例如黑洞解在此是爱因斯坦方程完全正则的解，质量 M 仅作为参数出现在解中。

In the second part of this chapter, we introduced dynamical scalar fields taking values in S^1 of circumference δ and winding once around the circle as it moves along a non-contractible loop on the manifold. Then, the matter action is minimized if the geometry of the manifold deforms in such a way that it is almost pinched, and the scalar field makes all its winding when passing through this region, as explained in section ”Dynamical Scalar Fields.” In the path integral, there is a competition between the matter action, which is minimized by pinched geometries, and the geometric action, which in turn is minimized by non-pinched geometries. A phase transition appears when the forced change in the scalar field winding around S^1 is large enough. In the new phase, the geometry is squeezed in some regions, which leads to an effective change in the topology from toroidal to simply connected one. The nature of this phase transition is certainly interesting to study because it is the first matter-induced phase transition in a higher-dimensional CDT. Moreover, the Monte Carlo results for the full CDT model are in agreement with the simplified minisuperspace model with a jump in the time direction, which also predicts a phase transition when changing δ .

在本章的第二部分，我们介绍了取值于周长为 δ 的 S^1 上，且沿流形上的不可缩回路运动时环绕该圆一周的动力学标量场。如“动力学标量场”一节所述，当流形几何发生形变至几乎被捏缩时，物质作用量达到最小，此时标量场在经过该区域时完成全部环绕。在路径积分中，偏好捏缩几何的物质作用量，与偏好未捏缩几何的几何作用量之间存在竞争。当绕 S^1 的标量场环绕的受迫变化足够大时，就会出现相变。在新相中，几何在部分区域被挤压，导致拓扑从环形有效变为单连通。该相变的性质非常值得研究，因为这是高维 CDT 中首个由物质诱发的相变。此外，完整 CDT 模型的蒙特卡洛结果与带时间方向跃迁的简化超空间模型一致，该模型同样预测改变 δ 时会发生相变。

Next, a dynamical three-component scalar field was introduced with the matching topological boundary conditions imposed based on three nonequivalent and non-contractible boundaries in the spatial directions, which can be defined for a globally hyperbolic spacetime with a toroidal spatial topology. We have established that such fields have a dramatic effect on the geometries that dominate the CDT path integral. This new kind of coupling between the matter field topology and the spacetime topology causes a phase transition for a strong enough coupling (a large enough δ in our model). In the new phase, the path integral is dominated by geometries with pinched regions, where the spatial volume fluctuates close to zero but is still connected due to kinematic constraints. This is shown in Figs. 16 and 17 for actual Monte Carlo configurations using coordinates given by classical scalar fields with nontrivial boundary conditions in non-contractible directions. Extrapolating this result to the large-volume limit, we obtain a picture with a small toroidal part of the cut-off size and a dominant geometry with a (nearly) spherical topology, as shown in Fig. 19. In conclusion, the impact of dynamical scalar fields is likely to be more important than previously expected and may have implications for the construction of cosmological models and even in other fields of physics related to phase transitions of topological nature.

接下来，我们引入了动力学三分量标量场，基于空间方向上三个不等价的不可缩边界施加了匹配的拓扑边界条件，这类边界条件可用于具有环形空间拓扑的整体双曲时空。我们已经证实，这类场对主导 CDT 路径积分的几何有显著影响。物质场拓扑与时空拓扑之间这种新型耦合，在耦合足够强时 (我们模型中对应 δ 足够大) 会引发相变。在新相中，路径积分由带有捏缩区域的几何主导，捏缩区域的空间体积涨落接近零，但受运动学约束仍保持连通。这一点在图 16 和图 17 的实际蒙特卡洛构型中得到了展示，我们使用了由不可缩方向上带非平凡边界条件的经典标量场给出的坐标。将该结果外推到大体积极限后，我们得到的图像是: 仅存在一个截断尺度的小环形部分，主导几何为 (近) 球面拓扑，如图 19 所示。综上，动力学标量场的影响很可能比此前预期的更重要，且可能对宇宙学模型，乃至物理学中其他与拓扑性质相变相关的领域有启发意义。

Cross-References

交叉引用

Semiclassical and Continuum Limits of Four-Dimensional CDT

四维 CDT 的半经典极限与连续统极限

- The Causality Road from Dynamical Triangulations to Quantum Gravity That Describes Our Universe

- 从动态三角剖分到描述我们宇宙的量子引力: 因果关系路径

Acknowledgments The author acknowledges support by the National Science Centre, Poland, under grant no. 2019/33/B/ST2/00589.

致谢作者感谢波兰国家科学中心在编号 2019/33/B/ST2/00589 资助项目下提供的支持。

References

参考文献

1. J.B. Hartle, S.W. Hawking, T. Hertog, Phys. Rev. D 77, 123537 (2008)

2. J. Ambjørn, A. Görlich, J. Jurkiewicz, R. Loll, Nonperturbative Quantum Gravity. Phys. Rept. 519, 127 (2012)

3. R. Loll, Class. Quant. Grav. 37, 013002 (2019)

4. J. Ambjørn, A. Görlich, J. Jurkiewicz, R. Loll, Int. J. Mod. Phys. D 22, 1330019 (2013)

5. J. Ambjørn, A. Görlich, J. Jurkiewicz, R. Loll, Phys. Rev. Lett. 100, 091304 (2008)

6. J.B. Hartle, S.W. Hawking, Phys. Rev. D 28, 2960 (1983)

7. K.G. Wilson, Phys. Rev. D 10, 2445 (1974)

8. J. Ambjørn, A. Görlich, J. Jurkiewicz, R. Loll, Phys. Rev. D 78, 063544 (2008)

9. J. Ambjørn, Z. Drogosz, J. Gizbert-Studnicki, A. Görlich, J. Jurkiewicz, D. Nemeth, Phys. Rev. D 94, 044010 (2016)

10. J. Ambjørn, J. Gizbert-Studnicki, A.Görlich, K. Grosvenor, J. Jurkiewicz, Nucl. Phys. B 922, 226 (2017)

11. J. Ambjørn, A. Görlich, S. Jordan, J. Jurkiewicz, R. Loll, Phys. Lett. B 690, 413 (2010)

12. J. Ambjørn, G. Czelusta, J. Gizbert-Studnicki, A. Görlich, J. Jurkiewicz, D. Németh, J. High Energ. Phys. 2020, 030 (2020)

13. J. Ambjørn, J. Gizbert-Studnicki, A. Görlich, J. Jurkiewicz, D. Németh, J. High Energ. Phys. 2019, 166 (2019)

14. J. Ambjørn, J. Gizbert-Studnicki, A.Görlich, J. Jurkiewicz, J. High Energ. Phys. 2014, 034 (2014)

15. J. Ambjorn, J. Gizbert-Studnicki, A. Görlich, D. Németh, J. High Energ. Phys. 2022, 103 (2022)

16. B.S. DeWitt, Phys. Rev. 160, 1113 (1967)

17. C. Rovelli, Phys. Rev. D 42, 2638 (1990)

18. J. Ambjørn, Z. Drogosz, J. Gizbert-Studnicki, A. Görlich, J. Jurkiewicz, D. Németh, Eur. Phys. J. C 81, 708 (2021)

19. J. Ambjørn, Z. Drogosz, J. Gizbert-Studnicki, A. Görlich, J. Jurkiewicz, Nucl. Phys. B 943, 114626 (2019)

20. J. Ambjorn, Z. Drogosz, A. Görlich, J. Jurkiewicz, Phys. Rev. D 103, 086022 (2021)

21. J. Ambjorn, Z. Drogosz, J. Gizbert-Studnicki, A. Görlich, J. Jurkiewicz, D. Németh, Class. Quant. Grav. 38, 195030 (2021)

22. J. Ambjorn, D. Coumbe, J. Gizbert-Studnicki, A. Görlich, J. Jurkiewicz, Phys. Rev. D 95, 124029 (2017)

23. J. Ambjørn, K.N. Anagnostopoulos, J. Jurkiewicz, J. High Energ. Phys. 1999, 016 (1999)

24. J. Ambjørn, J. Jurkiewicz, S. Bilke, Z. Burda, B. Petersson, Mod. Phys. Lett. A 09, 2527 (1994)

25. J. Ambjørn, Z. Burda, J. Jurkiewicz, C.F. Kristjansen, Phys. Rev. D 48, 3695 (1993)

26. J. Ambjørn, Z. Drogosz, J. Gizbert-Studnicki, A. Görlich, J. Jurkiewicz, D. Németh, Phys. Rev. Lett. 127, 161301 (2021)

27. A. Görlich, Introduction to Causal Dynamical Triangulations, in Quantum Gravity and Quantum Cosmology, eds. by G. Calcagni, L. Papantonopoulos, G. Siopsis, N. Tsamis (Springer, Berlin/Heidelberg, 2013), pp. 93-117

28. J. Ambjørn, A. Görlich, J. Jurkiewicz, R. Loll, J. Gizbert-Studnicki, T. Trześniewski, Nucl. Phys. B 849, 144 (2011)

29. K.V. Kucha, C.G. Torre, Phys. Rev. D 43, 419 (1991)

30. J. Ambjørn, T.G. Budd, J. Phys. A: Math. Theor. 46, 315201 (2013)